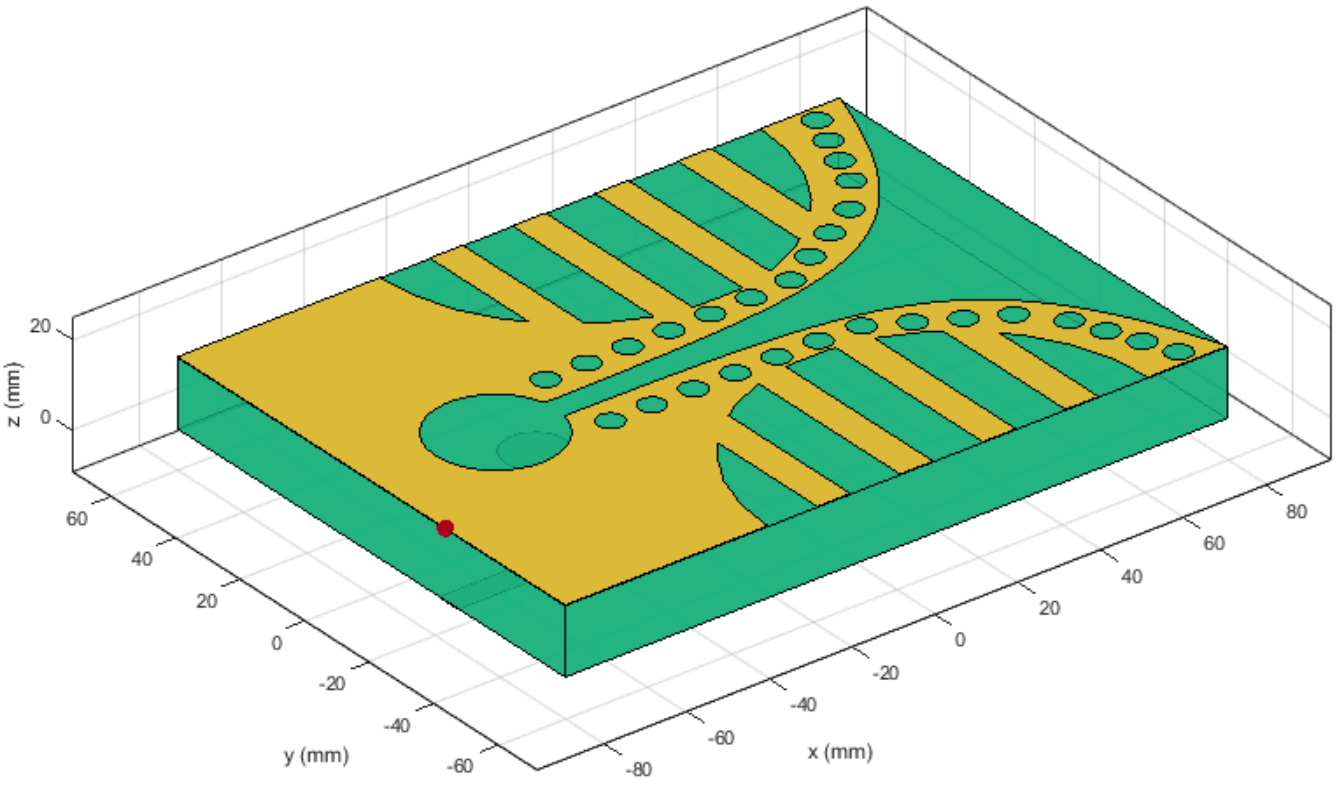

Real-time Snow Depth Measurement

Development and Construction of a System to Conduct Vehicle-Based Measurements of Snow Depth in Real-Time

Systems, Control and Mechatronics

Ask Olsson Uv

Lucas Rochard

DEPARTMENT OF MECHANICS AND MARITIME SCIENCES
CHALMERS UNIVERSITY OF TECHNOLOGY
Gothenburg, Sweden 2023
www.chalmers.se

Master's thesis 2023

Real-time Snow Depth Measurement

Development and Construction of a System to Conduct Vehicle-Based Measurements of Snow Depth in Real-Time

Ask Olsson Uv
Lucas Rochard

CHALMERS
UNIVERSITY OF TECHNOLOGY

Department of Electrical Engineering
Department of Mechanics and Maritime Sciences
Chalmers University of Technology
Gothenburg, Sweden 2023

Real-time snow depth measurement
Development and Construction of a System to Conduct Vehicle-Based Measurements of Snow Depth in Real-Time
Ask Olsson Uv
Lucas Rochard

Supervisor: Oskar Grankvist, CPAC Systems AB
Examiner: Peter Forsberg, Department of Mechanics and Maritime Sciences

Master's Thesis 2023
Department of Mechanic and Maritime Sciences
Chalmers University of Technology
SE-412 96 Gothenburg
Telephone +46 31 772 1000

Cover: Antenna PCB stack constructed in Matlab on both sides of a designed antenna on a dielectric FR4 substrate.

Typeset in LaTeX
Printed by Chalmers Reproservice
Gothenburg, Sweden 2023

Real-time snow depth measurement
Development and Construction of a System to Conduct Vehicle-Based Measurements of Snow Depth in Real-Time
Ask Olsson Uv
Lucas Rochard
Department of Mechanic and Maritime Sciences
Chalmers University of Technology

Abstract

This thesis presents a ground-based solution for measuring snow depth in real-time, specifically applicable to a vehicle. The primary motivation behind this study is the desire to enhance efficiency in snow-related domains through precise monitoring of snow depth. Typically, ground penetrating radars (GPR) have been used in conjunction with human operators to monitor ice and snow layers. However, this approach incurs costs in terms of both time and performance, leading to potential errors and uncertainties.

To address these challenges, this research explores the integration of artificial neural networks with GPR technology, aiming to boost their effectiveness in measuring snow depth. Various sensors, simulation methods, and neural network models were examined to develop high-performance solutions. Through extensive testing, a trained convolutional neural network achieved an accuracy of 1 cm on controlled experiments, showcasing the potential of combining these approaches. By enabling the system to conduct 20 depth measurements per second with this level of precision, a real-time solution for measuring snow depth is achieved.

Furthermore, the thesis proposes that incorporating the propagation speed of signals through the measured snow can further enhance the reliability of these monitoring systems. Such enhancements would provide valuable data to various fields that rely on accurate information about snow depth. By improving the overall efficiency and accuracy of snow depth measurements, this research opens up possibilities for advancements in snow-related domains.

Keywords: Ground Penetrating Radar, Snow depth, Neural network, Real-time, Dielectric, Antenna physics

Acknowledgements

We could like to extend our deepest gratitude to our advisor, Oskar Grankvist and examiner Peter Forberg for the help and constructive criticism of this thesis. We would also like to thank Skidome for allowing us to perform our experiments and test at their facilities. Kudos to Nordconsult for the help of lending a ground-penetrating radar on which we could gather data. Credit for the help with the antenna production goes to the help and professionalism of TeknologTryck at Chalmers. Lastly, thanks to CPAC Systems AB for supplying the tools, help and support during this thesis.

Ask Olsson Uv & Lucas Rochard, Gothenburg, June 2023

Thesis advisor: Oskar Grankvist, CPAC Systems AB
Thesis examiner: Peter Forsberg, Department of Mechanics and Maritime Sciences

List of Acronyms

Below is the list of acronyms that have been used throughout this thesis listed in alphabetical order:

ANN	Artificial Neural Network
C.E.S.A.-GPR	Cost-Effective Self-Assembled Ground-Penetrating Radar
CNN	Convolutional Neural Network
GPR	Ground Penetrating Radar
LF	Low Frequency
LiDAR	Light Detection and Ranging
MILP	Mixed-Integer Linear Programming
NDT	Non-destructive testing
PCB	Printer Circuit Board
PML	Perfectly Matched Layer
PoC	Proof of Concept
RADAR	Radio Detection and Ranging
RF	Radio frequency
TLS	Terrestrial LiDAR scanning
ToF	Time of Flight
UAV	Unmanned aerial vehicle
UWB	Ultra Wideband

Nomenclature

Below is the nomenclature of variables that have been used throughout this thesis.

Variables

B	Bandwidth [Hz]
f	Frequency [Hz]
f_H	Upper frequency of a signal [Hz]
f_L	Lower frequency of a signal [Hz]
f_c	Central frequency of a signal [Hz]
B_f	Fractional Bandwidth
B_r	Ratio Bandwidth
λ	Wavelength [m]
ε	Dielectric permittivity
σ	Electric conductivity
μ	Magnetic permeability
q	Charge density $[C/m^3]$
$\vec{J}$	Current density $[A/m^2]$
$\vec{E}$	Electric field $[V/m]$
$\vec{B}$	Magnetic induction [T]
$\vec{D}$	Electric displacement $[C/m^2]$
$\vec{H}$	Intensity of Magnetic field [A/m]
v_p	Propagation velocity [m/s]
c	Light celerity [m/s]
$e_{simulated}$	Normalised error of simulated data
e_{real}	Normalised error of real-world data

Contents

List of Figures

List of Tables

1
Introduction

In recent decades, a significant part of the population's interest in the weather and its impact on daily life has grown. Recurrent problems arise every winter due to the presence of snow. Substantial amounts of money and time are invested in its removal or displacement[1]. Precise gauging and monitoring of snowpacks have gained significant importance in different fields, such as meteorology, climate science, environmental studies, and disaster prevention. Understanding snow covers' spatial distribution, density, and moisture content is crucial for many reasons. It aids in predicting avalanches, managing water resources, assessing climate change impacts, optimising transportation systems, and even studying winter ecosystems' ecological health[2]. The measurement of snow depth and its characteristics has been a longstanding research topic in these disciplines[3].

Various methods have been explored and utilised to determine snow depth, from traditional manual measurements[4] to advanced remote sensing techniques[5]. These remote methods include but are not limited to, ground-based measurements, weather station data, satellite observations, and modelling combined to provide comprehensive insights into snowpacks. However, no single method offers a complete solution, as each has its own advantages and limitations. Ongoing research focuses on improving snow depth measurements' accuracy, efficiency, and real-time capabilities. Research in sensors and monitoring systems aims to provide continuous and precise information about snowpack and their layers. These innovations enhance the understanding of snow accumulation, improve forecasting models, and support decision-making processes related to winter weather conditions. Expanding the knowledge of snowpacks and their characteristics improves adaptation to manage the various impacts associated with snowfall, such as transportation disruptions, flood risk assessments, energy management, and the overall resilience of winter ecosystems[6].

The study of snow covers plays a crucial role in understanding the weather's influence on the environment at large. Accurate measurement and monitoring of snow depth and its characteristics contribute to improved safety, resource management, and overall resilience in the face of changing winter conditions. There is an interest in developing real-time solutions to measure snow depth to facilitate the topics mentioned above.

1.1 Research questions

The following topics were deemed of importance and the beginning of the thesis:

- What sensors are viable for the measurement of snow depth in real-time?
- How is it possible to, in real-time, apply these sensors to measure snow depth in a robust manner?
- How is it possible to automatically process the data into snow depth measurements?

1.2 Methodology

This master's thesis aims to investigate the feasibility of various sensor types for real-time snow depth measurements. The study will delve into techniques for interpreting and extracting relevant information from the collected data, focusing on enhancing the accuracy of these interpretations. Furthermore, the research will explore the processing of sensor signals and examine the potential application of machine learning techniques, specifically artificial neural networks (ANN), to optimise the outcomes of snow depth measurements.

To reach this goal, quantitative studies of different sensors method will be explored first to narrow the field of study progressively. After reaching a consensus about which sensor or sensors are of interest, a qualitative study will be presented, giving necessary knowledge of the chosen sensor and how it can be used. The type of data obtainable from the sensor then needs to be analysed to determine which process will be applied to it, from filtering to transforming. Different machine learning networks will be researched to determine the best way to obtain precise sensor depth data. After reaching satisfying simulation results and proof of concept, the possibility of performing real-world tests is to be explored. At a later stage, improvements upon these tests and theories to develop the project further will be proposed.

1.3 Scope and limitations

The studied problems will explore sensors from which depth or similar data can be extracted. Types and densities of snow and their effect on signals will be of interest, restricted to what is available in Gothenburg for the Januari-May period. Indirect snow-depth measurements and analysis of snow composition or static solutions will not be further expanded due to the wish to develop a solution capable of working independently from outside data sources. In this study, the relevant depths to measure range from directly below the surface up to 150 cm since further depth is not relevant to the purpose of this thesis. Real time is defined as solutions exceeding 10Hz based on desires from CPAC.

Due to hardware restrictions, only the frequencies presented in the thesis are tested, resulting in a restricted frequency study.

2
Theory

2.1 Electromagnetic waves

Electromagnetic fields are characterized by moving electric charges; therefore, the forces applied are all vectors. They can generally be described by four equations called Maxwell's equations, defined as follows:

$$\nabla \times \vec{E} = -\frac{\partial \vec{B}}{\partial t} \tag{2.1}$$

$$\nabla \times \vec{H} = \vec{J} + \frac{\partial \vec{D}}{\partial t} \tag{2.2}$$

$$\nabla \vec{D} = q \tag{2.3}$$

$$\nabla \vec{B} = 0 \tag{2.4}$$

The first equation characterizes Maxwell's expansion upon Faraday's law defining the creation of electrical fields $\vec{E}$ through changes in magnetic fields $\vec{B}$. Equation (2.2) defines the effect that is brought by changes in electrical displacement $\vec{D}$ and currents $\vec{J}$ in the generation of circulating magnetic fields $\vec{H}$. Equation (2.3) expresses the difference between the electrical displacement $\vec{D}$ and its charge q. Lastly, equation (2.4) explains the non-existence of isolated magnetic poles $\vec{B}$ and attraction between said poles.
These equations further explain how electromagnetic waves travel through different mediums:

$$\vec{J} = \sigma \vec{E} \tag{2.5}$$

$$\vec{D} = \varepsilon \vec{E} \tag{2.6}$$

$$\vec{B} = \mu \vec{H} \tag{2.7}$$

Equation (2.5) refers to Ohm's law applied to physics where a current's density $\vec{J}$ is directly dependent on the conductivity σ of the medium and its electric field $\vec{E}$. Electric displacement $\vec{D}$ of a magnetic wave depends on an electric field's intensity $\vec{E}$ and a travel medium's dielectric constant ε according to equation (2.6). Magnetic induction $\vec{B}$ is, in turn, dependent on the intensity of a magnetic field $\vec{E}$ in relation to the permeability μ of the medium. These equations then allow for calculating the propagation speed of waves through a specific medium:

$$v_p = \frac{c}{\sqrt{\varepsilon}} \tag{2.8}$$

Electromagnetic waves normally travel at the speed of light, but materials that affect waves reduce this speed depending on their permittivity and dielectric constant. Travel time of electromagnetic waves is then given by twice the length of the medium and their propagation speed as:

$$t_t = \frac{2L}{v_p} = \frac{2L\sqrt{\mu\varepsilon}}{c} \tag{2.9}$$

In the end, depth can be determined as:

$$depth = \frac{t_t}{2}\frac{c}{\sqrt{\varepsilon}} \tag{2.10}$$

In the electromagnetic wave application studied by the thesis, most materials have a permeabillity, μ, value close to one, simplifying equation (2.10)[7].

2.1.1 Dieletric

A material is said to be dielectric when it has insulating properties. Very little current flows in them when exposed to electric fields. They affect electromagnetic waves through polarization; hence, electrical charge is reduced in their presence. On the other hand, energy storage capacity increases. Therefore, the dielectric constant of a material indicates how insulating the material is, and permittivity indicates how much energy can be stored in it.

2.1.2 Wave propagation

Two general types of waves can be identified, mechanical and electromagnetic. The first one requires a physical medium to travel. For example, sound needs air or material to propagate through, such as the motion of water transmitting surface waves. The second type doesn't require a medium and can be propagated through a vacuum, for example, light and radiowaves, which are electromagnetic radiation functioning at different frequencies. Waves are subjected to many mechanics when propagating. The following four mechanics are relevant to the thesis: Reflection, refraction, diffraction and interference.

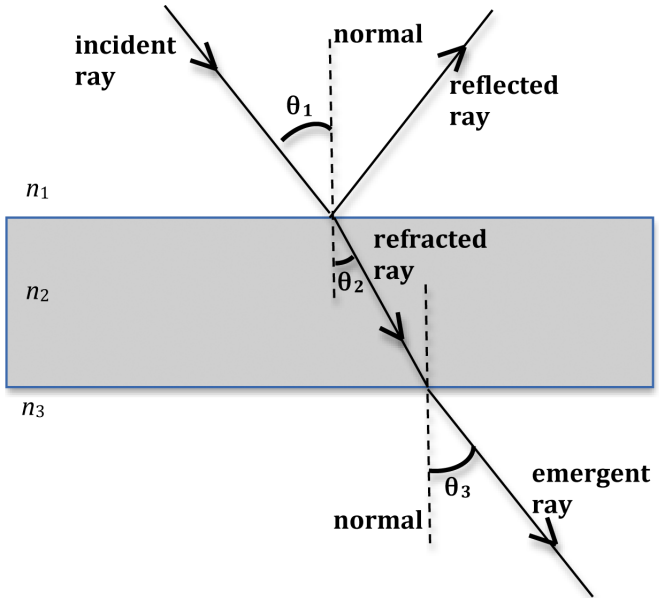

Figure 2.1: Diagram illustationg reflection and refraction of light

The phenomenon of a wave reaching an obstacle and bouncing back is called reflection. The angle at which a wave is reflected directly depends on the angle at which it encounters an obstacle, as seen in Figure (2.1)[8], θ_1 will be ported on the reflected ray. For refraction, different materials possess different refraction indices that are dictated by a ratio between the speed of light in a vacuum and the speed of light in a traversed medium. The angle is then dependent on the angle of incidence and the refraction index of the medium. The propagation angle is modified when a wave encounters an obstacle with a small hole or small obstacles. That is called diffraction; see Figure (2.2)[9].

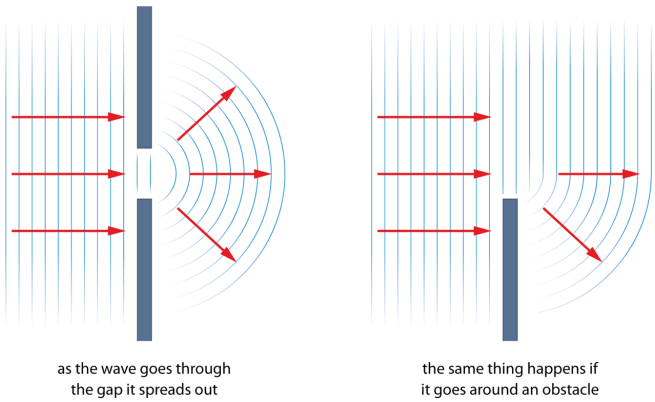

Figure 2.2: Diagram illustrationg diffraction in light

The last case is interference. When two or more waves come in contact, they will affect each other if their peaks happen simultaneously. If they are in the same phase, waves will strengthen each other, but if they are phase-reversed, depending on how much energy the waves hold, they will dampen themselves or cancel out each other if their energy is similar.

A wave's energy is affected by reflection on materials, depending on the angle and the polarization of an obstacle with the relation:

$$\frac{obstacle - air}{obstacle + air}^2 \tag{2.11}$$

The polarization can add an angular parameter[10].

2.2 Radars: A general theory

Radar, an acronym for radio detection and ranging, are sensors that detect positions over diverse ranges through diverse physical and digital radio wave techniques. These techniques will affect the radar's main properties: frequency, bandwidth, accuracy, and range. Radars transmit and receive electromagnetic waves to function, measuring distance through the reflection of radiowaves.

In a vacuum, electromagnetic waves travel at the speed of light, c, so the distance to the measured target where reflection happens is defined as:

$$R = \frac{ct}{2} \tag{2.12}$$

where t is the wave's travel time, and the division by 2 is because the one-trip distance is regarded. A radar consists of a transmitter generating the radio-frequency pulse with the required characteristics for each radar. Then a receiver captures the echo and amplifies it to make it detectable and able to be processed by radar. In order for waves to be sent and caught, specific antennas are developed. By changing these components, their size, working frequency and many other electrical parameters, different radars can be designed suited to specific tasks. Certain designs are better suited for detecting objects at shorter ranges or through materials. Others are better for detecting moving objects at longer distances.

2.2.1 Bandwidth

Bandwidth, in this context, refers to the term used in signal processing and is defined as an interval of frequencies defined in hertz. It indicates the size of a signal's frequency range and is determined by the difference between its upper and lower frequency:

$$B = f_H - f_L \tag{2.13}$$

Information carried by bandwidth is not dependent on frequencies at which the bandwidth lie; it is constant. Equation (2.13) is used for theoretical calculations of bandwidth but not to determine the properties of an antenna. Instead, the relative bandwidth is used. It can be defined as either the fractional bandwidth or the ratio bandwidth. Fractional bandwidth is defined as the theoretical bandwidth divided by the mean of the upper and lower frequencies called the central frequency f_c[11]:

$$B_f = \frac{B}{f_c} \tag{2.14}$$

While the ratio bandwidth is defined as the ratio between the upper and the lower frequency:

$$B_r = \frac{f_H}{f_L} \tag{2.15}$$

2.2.2 Antennas

Antenna design is of high importance in the design of radar as it transforms electrical signals into electromagnetic waves. There exist many types of antennas, and they vary in size, shape as well as material. Their design plays a crucial role in determining their operating frequency, range, bandwidth, and effective gain. These factors are influenced by the antenna's length, angles, and shape, which determine how the electromagnetic waves will bounce. The wavelength of a signal is a determining factor of the length of an antenna:

$$\lambda = \frac{c}{f} \tag{2.16}$$

The length of an antenna can be a multiple of its wavelength. For optimal theoretical use of an antenna, the full wavelength is recommended. Dividing its size by two or four also give resonance for the chosen frequency. In practice, one can therefore reduce the size of an antenna to give resonance at other frequencies than the fundamental frequency, especially in wideband applications[12]. Common antenna designs include[13]:

- Aperture: Antenna with an opening used to direct its signal and increase its gain. Often used on air- or spacecraft.
- Array: Group of small antennas cooperating to produce a single radiation pattern. It provides an increased gain, reduces interference, and improves the directional propagation of waves. This system is often used in communication systems, 5G networks and military systems
- Lens: An antenna using an integrated glass or dielectric lens, making use of optical properties to amplify the frequency. It is common in radar and microwave systems.
- Log Periodic: An antenna composed of elements supporting a broader frequency range, arranged in a logarithmic shape. They are used for systems needing variable bandwidth or high-frequency communication. This includes analogue television, cellular communications or shortwave radio.
- Microstrip: Small antenna printed on a circuit board. Used in wireless communication systems or mobile devices.
- Reflector: Antenna including components that reflect waves to focus or direct them. Used in microwave or satellite communications, often including a parabolic structure.
- Travelling wave: A directional antenna where waves only travel in one direction, enabling a wide frequency range. They are mainly used for analogue television, amateur radio and telecommunications.
- Wire: An antenna made of a wire connected to a transmitter or a receiver making it useful in transport systems, radios, and buildings.

2.2.3 Types of radar

- **Pulse Radar**: A pulse radar sends short, high-energy radar pulses to measure the travel distance when the pulse has travelled back to the radar. They are mostly used to measure objects at very far distances.
- **Continuous wave radar**: A continuous wave radar sends continuously processed radar signals, leading to permanent information on the target being measured. They are used to have a constant position of a measured target, like a ball flying through the air.
- **Ultra wideband radar**: Ultra wideband radars use frequency spectrums that are very large and exchange more data at the same time than conventional narrowband radars. The waveform changes, due to the bounces, does not affect these radars much. They are, therefore, used to detect positions through obstacles or in the ground.

2.2.4 Processing radar signals

Many mathematical methods are available to process radar signals that allow for specific information to be obtained, such as filtering to remove noise and emphasise the target of measure. The distance measured by radars is not directly extractable as the medium in which the waves travel affects how long it will take for an echo to bounce back. These signals are usually studied manually to determine distance, but methods, such as neural networks, are starting to be applied instead.

2.3 Physical and chemical properties of snow

Snow is largely constituted of water and air, tending to ionize easily and affecting light and other waves that travel through it[14]. It also has electrical properties that vary depending mainly on the type of snow and its temperature[15].

2.3.1 Electical properties of snow

The water molecules in snow tend to ionize and give up their two hydrogen electrons, thus generating electric charges. How these charges arise, and their direction and organization contribute to separate electrical properties. The orientation of water molecules due to ionization is largely responsible for the permittivity characteristic.

The temperature and hydration, that is, the fluid water content of snow, have a large role to play in these relations. Generally, a lower snow temperature will decrease its permittivity while increasing the speed at which waves travel in it[16]. Snow has been measured to have a conductivity of around $0.01\frac{\mu S}{cm}$[17].

2.3.2 Optical properties of snow

Snow reflects, refracts, and absorbs electromagnetic waves according to their properties, which affects measurement based on optical data. Absorption of electromagnetic waves is done by different mechanisms depending on the wave's place in the

spectrum. Due to its electrical properties, snow absorbs small wavelengths, such as ultra-violent light (UV); the molecular vibrations will absorb larger wavelengths in the infrared spectrum. Snow, a mix of water in a solid state and air, is a highly reflective and refractive material. Light is, therefore, easily scattered and loses its strength and some of its wavelength when passing through the snow.

2.3.3 Snowpack stratigraphy

The understanding of snow layer evolution plays a role in sensor calibration. Snow covers develop during longer periods and form layers with different properties, called snowpack stratigraphy. This domain is influenced mainly by weather, temperature, wind, and atmospheric pressure. Different densities and snow temperatures lead to different electromagnetic and optical properties, so their understanding is needed to suggest credible theories and simulations[18]. Taking the example of glacier formation, it is possible to represent the layer formed throughout hundreds of years, illustrated in Figure (2.3)[19]:

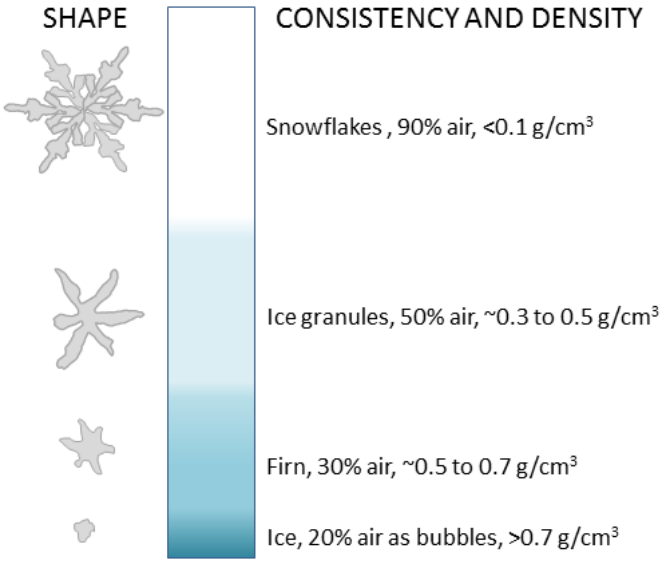

Figure 2.3: Formation of glacier ice layers

As the amount of air in snow decreases, the dielectric constant will decrease. A higher amount of water will increase the dielectric constant. Deeper snow leads to less water being present in liquid form as snow layers are heavily packed, colder and less exposed to heat from the surrounding air and sun rays. The type of layers and their electrical properties follow a general pattern, and whilst different conditions change these properties, there is, in general, little deviation when compared to other materials.

2.4 Artificial neural network

Artificial Neural Networks, henceforth ANN, have become increasingly popular in recent years as a valuable solution for tackling complex challenges in different fields. ANNs are modelled after the human brain's structure and functionality, offering a computational structure to learn and make intelligent decisions based on data. There are many different types of ANNs, and they each apply to different fields or problems.

2.4.1 General concept of an ANN

At the core of an artificial neural network lies the neuron, the fundamental building block. The neuron mimics the behaviour of a biological neuron by receiving inputs, processing them, and producing an output. It operates through a combination of activation functions, weights, and biases. The activation function introduces non-linearities into the network, enabling it to learn complex relationships and make non-linear decisions. The weights and biases determine the strength of connections and the neuron's influence on the overall network output.

2.4.2 Fully connected ANN

A fully connected ANN or dense ANN is also known as a network structure with full connections between neurons. These networks are the most basic types of networks[20]. The input is split up and fed directly into each neuron. Each neuron then only looks at that part of the input and learns whether it should return a high or low signal overtraining. The output of these neurons is then fed into a second neuron layer that continues to give output signals depending on how the desired results look. In between layers, there can be separate processing to create robustness in the network. Dropout is an example of this. In a dropout layer, a determined percentage of the neurons' signals are randomly and synthetically lost. The following layer of neurons learns to classify the data even if some parts go missing.

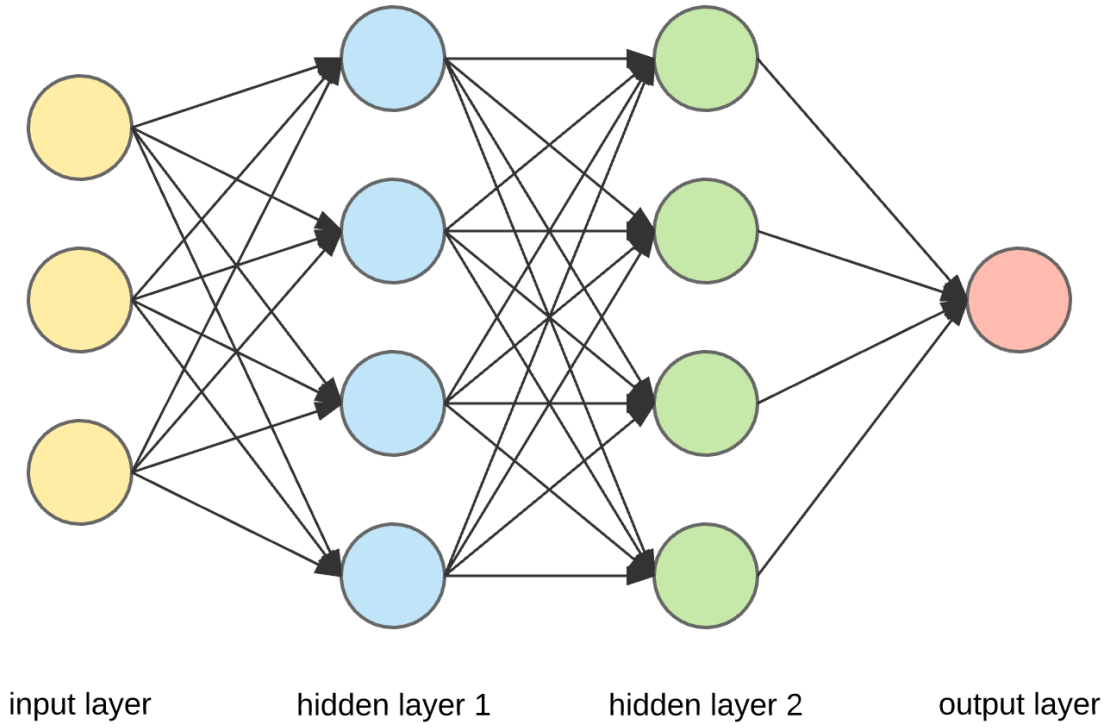

Figure 2.4: Example structure of a dense ANN

Dense ANNs grow exponentially in complexity, and computational requirements as more layers and neurons are added, illustrated by the arrows in Figure (2.4)[20]. This makes the network slow to train and, since each input part is handled separately, more susceptible to noise and outliers.

2.4.3 Convolutional ANN

A convolutional neural network (CNN) is a specialized network architecture designed to consider the values of neighbouring neurons. It achieves this by applying a convolving filter over the input, allowing each neuron to gather information from a wider region of the input data as shown in Figure (2.5)[21]. In contrast to a dense neural network, where neurons are fully connected, the neurons in a CNN send their signals to another layer that applies convolutions, enabling the network to acquire a broader understanding of the input data.

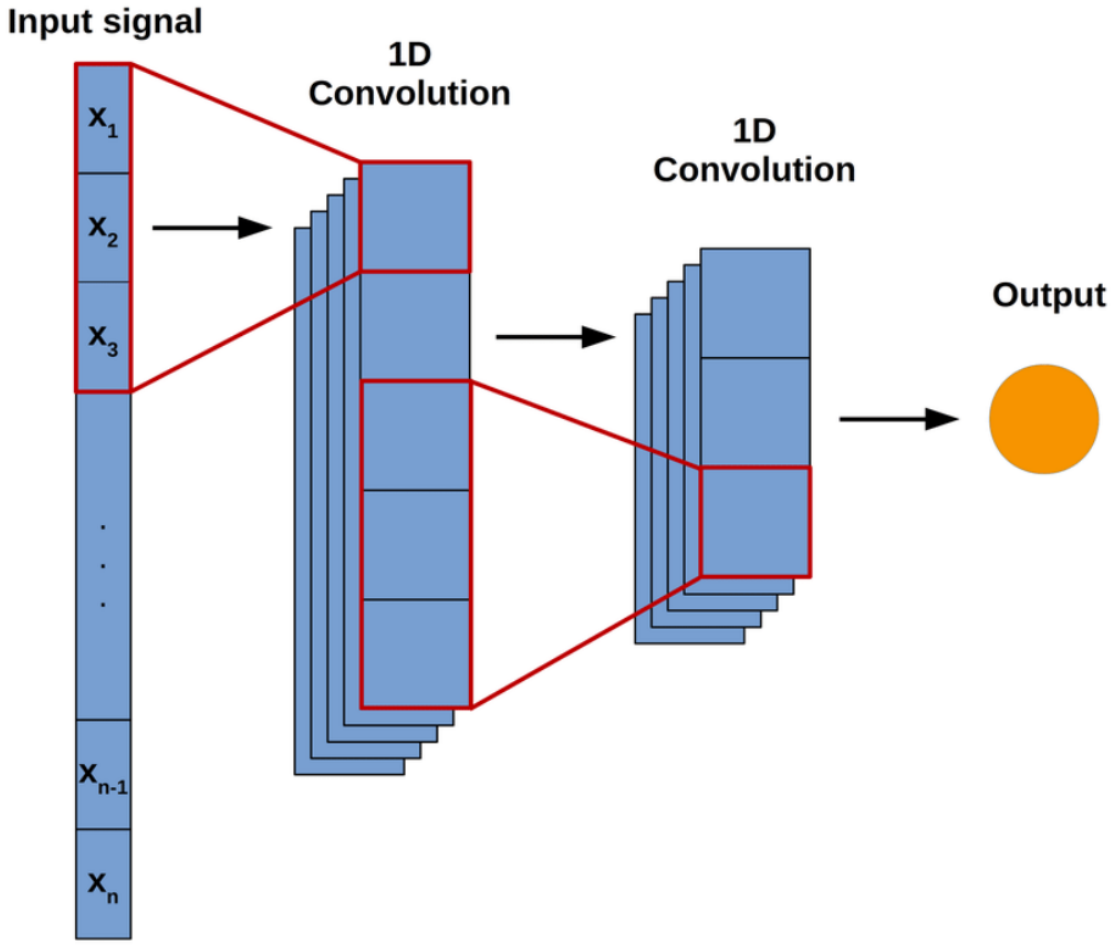

Figure 2.5: Example structure of a one-dimensional CNN

A CNN excels at extracting and detecting features within the input by employing convolutions. It learns to identify distinctive patterns and responds differently based on the presence or absence of these features. This characteristic empowers CNNs to exhibit robustness, focusing on recognizing features rather than specific numerical segments of the input. Consequently, CNNs require fewer parameters than dense neural networks, making them more efficient in terms of computational resources while still achieving impressive performance.

2.4.4 Training of a neural network

When constructed, a network needs to be trained to make predictions. This involves presenting input data with a known label, henceforth annotated data, and giving them to the network. After predicting these, the output is compared against the actual labels to acquire an accuracy score of the network. The network then adjusts weights and biases in its nodes to acquire better accuracy. How these weights are adjusted can be done in many ways, the most common way is backward propagation. Other optimization methods, such as biologically inspired methods, can also train a neural network[22]. These optimisation methods can avoid local optimums that backward propagation could converge to instead of finding the optimal solution.

3
Methods

A literature study, presented throughout the thesis, was performed to find information on the research questions reliably and effectively. Better information entails better choices for the development of the thesis. To facilitate information collection, each reference read was documented with information about general topics, findings and relevance of the reference. This allowed for easy filtering of the references and their information later in the writing. The main research points explored in this section were:

- Different sensor types and their interaction with machine learning to process the signals
- Physical properties of snow and how they interact with electromagnetic waves
- Ways to simulate and extract data from different sensor types

3.1 Choice of sensor

Sensor selection is crucial in acquiring accurate measurements of specific targets. This involves considering the properties of the material or target being measured. Obtaining relevant information about the material is essential in making relevant choices when it comes to selecting sensors. Sensors offer a broad range of options for data acquisition, available in various shapes and sizes, with wide-ranging applications. Exploring and evaluating different types of sensors is essential in the context of measuring snow depth. This analysis aims to identify the most suitable solution for the given problem. By examining common sensor types and their potential applications, a sensor for snow depth measurement will be forthbrought.

3.1.1 LiDAR

LiDAR stands for light detection and ranging. The technology is similar to RADAR's, but near-infrared light waves are used instead of radio waves in this specific case.

Different kinds of LiDARs where the medium used to send and receive the wave and its processing differ slightly[23]. The main idea behind a LiDAR is to send out a laser and measure the time of flight or the alteration of the light signal when received and extract the sought-after information, illustrated in Figure (3.1).

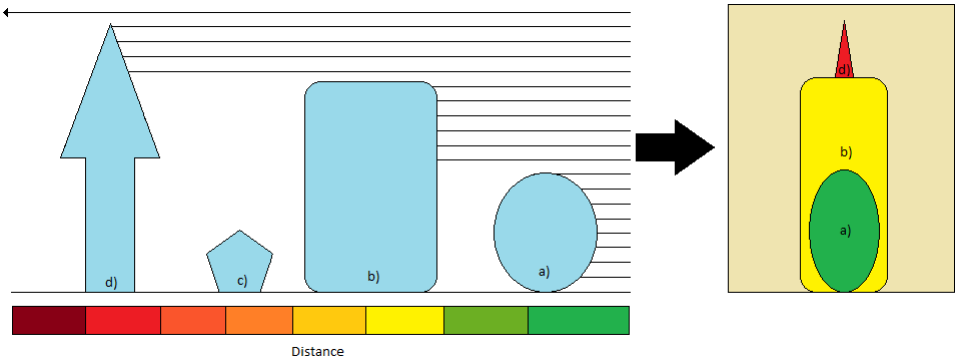

Figure 3.1: Diagram of the LiDAR principle. The measured area is the left side, with the LiDAR pointing in that direction. The right side is the LiDAR output. Laser beams are projected on an area, and the time it takes for these lasers to return gives both the location of the object and the distance to said object. Notice here how object c) is not visible in the output since no laser rays were able to hit it.

This process is subject to noise depending on the medium the light passes through or physical noise in the sensor's construction[24]. It is possible to get an accurate position of the measured LiDAR space and therefore create mappings of the studied area. Usually, large regions are scanned with the help of motor-mounted heads on the LiDAR, obtaining the position where the beam is reflected. Its use has seen an increase in popularity and several applications. It is nowadays common to be found for distance analysis, for example, in cars[25] or research made in archaeology[26].

A particular application of LiDAR called terrestrial LiDAR scanning exists, henceforth TLS, specializing in topographical model creation through the use of LiDAR technology[27]. It has diverse applications for archaeological studies and meteorological and terrain evolution.

LiDAR allows for scans in one to three dimensions depending on how the beam is being sent out and the wavelength of the laser, ranging from 200-2000 nm.

Solutions incorporating LiDARs in snow-depth measurements have been researched and are used commonly coupled with GNSS positioning. The process includes comparing the position of the reflection of the LiDAR beam on the snow to a highly accurate mapping of the measured area made by different means, for example, GNSS or other LiDAR mappings[28][29]. The use of LiDAR in snow-depth measurement is often not applicable in real-time as values need to be compared to models. The values obtained can be highly accurate and encompass large areas simultaneously[30]. Airborne mappings and analysis using LiDAR are still the most common uses of LiDAR when it comes to snow depth measurement, as the accuracy obtained by UAVs is good.

However, LiDAR beams can't function correctly after permeating the snow due to significant scattering of light rays or loss of power and wavelength absorption, as referenced in the theory section 2.3.2. This means that the measurement of snow depth always has to be made through a comparison with a previous measurement or map that might have changed if the terrain has deteriorated. This is very time-consuming and hinders the deployment of a system in a new environment.

The goal of the problem at hand is to measure snow depth in real-time where no previous knowledge of the terrain is necessary. In that aspect, LiDAR is not a good choice since it is incapable of that, but it is a relevant and qualified choice for measurements not happening in real-time.

3.1.2 Ultrasonic sensors

Ultrasonic sensors emit sound waves at frequencies inaudible to the human ear, from 25kHz. A common high-frequency application is medical imaging using ultrasounds ranging from 3-10 mHz. Sound is propagated by creating movement in the air particles transmitting waves at a decided frequency. It is, therefore, subject to noise due to changes in the transmitting medium. Ultrasonic sensors are the most common sensors found using sound as a medium. They are mainly used for distance calculations, measuring the Time of Fligt, henceforth ToF, between sending and receiving the signal[31]. Being relatively cheap and accessible, they are popular for home projects and more affordable prototypes or use on Arduino[32]. A practical model can be accessed from 2000 SEK. Ultrasound is a widely researched topic due to its numerous applications[33].

Several applications of ultrasonic sensors to measure snow depth have been tested[34][35][36]. Most applications are found to be static, giving a periodic evolution of the depth under the sensor. Such sensors usually send a pulse, receive the echo, and measure the time difference. Several echos will be observed when measuring snow depth, so the time difference between the different echos is what is regarded and calculated, giving a distance based on the speed of sound in the measured material.

As explained in the studies, cold and wind affect ultrasonic measurements and can even render the data unusable in short intervals during heavy snowfall. Suppose the snow depth measurement happens at temperatures that vary a lot, as well as being exposed to heavy snowfall or snow movements, for example, driving a snowmobile. In that case, the measurements will become more inaccurate. Moving while measuring also proves to be a challenge since the echo will constantly have to compensate for the change in position.

It is a suitable choice for a cheap, static real-time sensor, but the limitations and drawbacks are responsible for a very restricted case if it is chosen. The possibility of moving or exposing the sensor to harsh conditions is high, posing a risk in data processing.

3.1.3 Radars

Radar is a general group of sensors using the transmission and reception of radio waves through a medium to extract information like the distance and angle measured[37]. Many types of radars exist depending on how the radio wave is being sent out and processed.

3.1.4 Synthetic-Aperture Radar

Synthetic-aperture radar, SAR for short, is a radar that utilizes its own movement to create high-precision 2D or 3D reconstructions of large-scale terrains such as mountains, landscapes, and even planets. It is usually mounted on aeroplanes, satellites, or other spacecraft. The general principle is that of a regular radar. It sends out radio pulses and measures the time it takes to receive them back. The movement of the SAR is key to achieving high-fidelity spatial resolution compared to station-basted radar scans. The name synthetic aperture comes from the seemingly larger antenna aperture. The SAR achieves the antenna size by moving into a new position and receiving its previously sent radar signal. In general, the larger the antenna, the higher the resolution of the scans[38].

In snow depth measurements using SAR, the depth is measured by the delay of the radio waves when travelling through the snow as opposed to the reflection from the snow surface, see Figure (3.2). Since the antenna is synthetically large, this measurement yields a good measurement value close to the ground truth. However, this does not work when applied to a ground-based approach. This makes the sensor setup expensive, and the measurements are not on demand. One would have to wait until the satellite or aircraft is nearby before doing measurements[39].

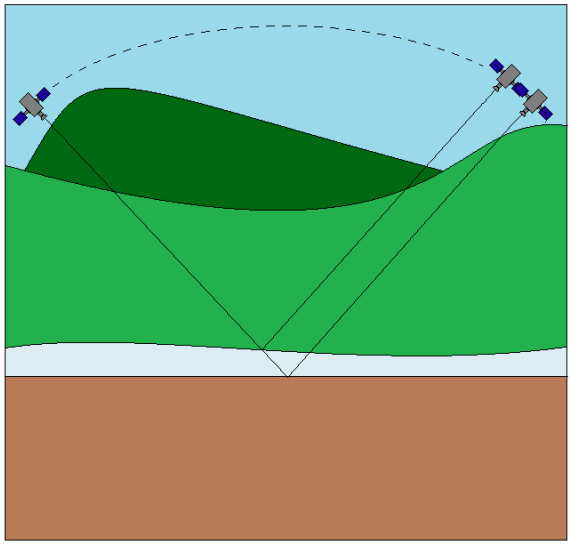

Figure 3.2: Illustration of a SAR measuring snow depth

3.1.5 Ground penetrating radar

Ground penetrating radar, henceforth GPR, is a specialized application of radar technology. It works by emitting high-frequency electromagnetic wave pulses and measuring the time and wave distortion of the received reflected waves. With the time and shape of the received waves, it is possible to conclude how far away an object is and what material properties said material has. GPR sensors have large applications in non-destructive testing, henceforth NDT. Knowing the return time and change in wave properties, one can apply Maxwell's equations (2.1)-(2.4) to be able to measure the distance to an object or material. The GPR penetrates materials from ice and snow to concrete and bedrock using high-frequency electromagnetic waves. The penetration ability of the GPR is frequency dependent. An increase in frequency yields a decrease in wavelength, narrowing the viewing range. For ice and snow applications, a frequency of 250-500 MHz is commonly used[40]. A higher

frequency leads to shallower but more exact measurements and is less susceptible to outside forces. Snow and ice have less energy absorption than other common materials, so higher frequencies can be used. The response and shape of the waves received back are determined by the distance to the object and the object's dielectric constant, which is the material's ability to store electrical energy.

There are two common applications for the GPR, either ground-coupled or air-coupled. Ground-coupled usage of the GPR regards the use of a GPR dragged or rolled along the ground. This is mostly used in applications where the thickness of pavement and ice sheets, among other things, are measured and the accessibility for a ground vehicle is feasible[41]. Air-coupled is mainly used for wild-land measurements where the accessibility of ground vehicles is low[42]. The main difference between these two is that the ground-coupled measurements always show the ground surface at the height zero and looks flat, while air-coupled shows the variations in terrain such as hills and valleys.

A GPR can provide data in three processing stages, A-, B-, and C-scans. A-scans consist of a single pulse measurement where the received wave can be interpreted. This type of scan gives a 1-dimensional measurement of the subsurface properties below.

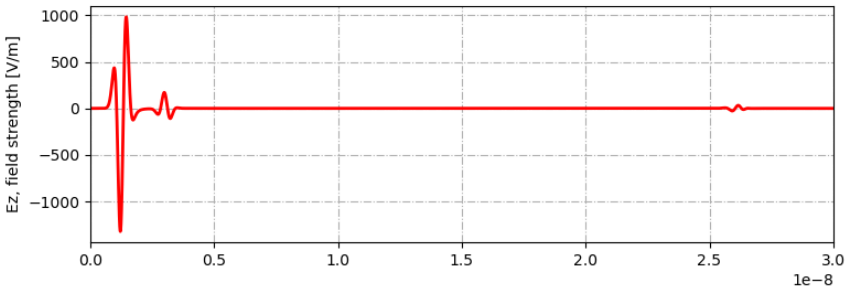

Figure 3.3: A-scan simulated using gprMax where the x-axis denotes the response time. The first reflection is the radar waves bouncing against the top layer of soil, and the second, smaller reflection is a subsurface detail.

B-scans consist of multiple A-scans in series and can be interpreted as a 2-dimensional measurement or "slice" of the subsurface, illustrated in Figure (3.4).

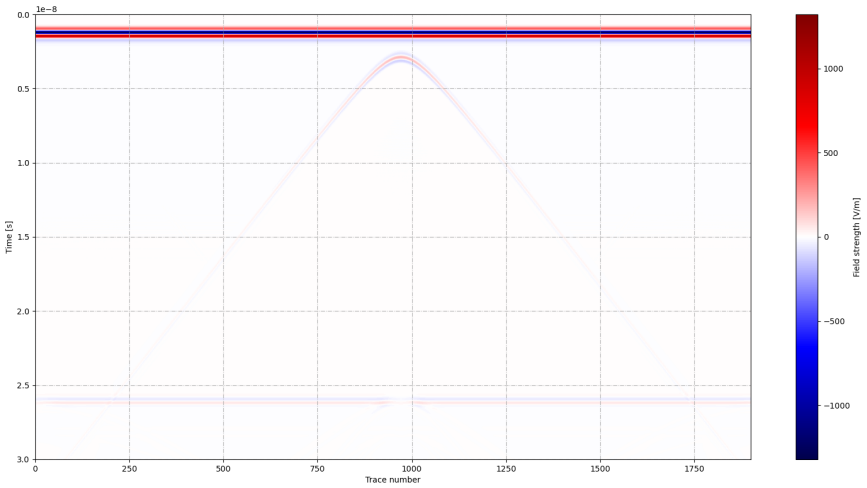

Figure 3.4: B-scan simulated using gprMax where Figure (3.3) is taken at trace 950

Finally, C-scans, as the one in Figure (3.5), consist of multiple B-scans in parallel and give a 3-dimensional representation of the subsurface[43].

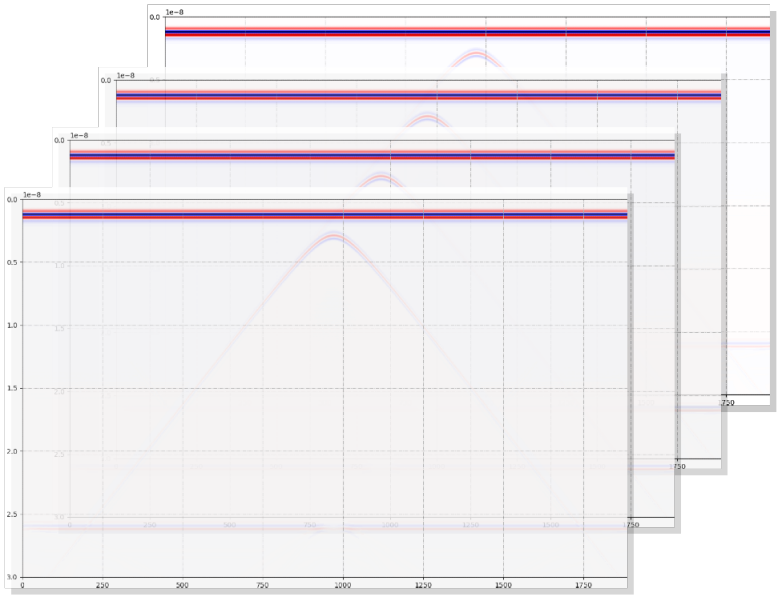

Figure 3.5: C-scan illustrated using gprMax B-scans, this scenario depicts a steel pipe in soil.

For the measurement of snow depth, there are some factors to consider. Firstly, since the solution aims to be applied in real-time and mounted on a vehicle, the air-coupled version of the GPR is unsuitable as it would require an additional vehicle to synchronize and exchange information. When measuring snow depth, there will

be noise in the form of sound from the snow machine, wind, and snow particles in the way. All of these obstacles disappear with the GPR as the electromagnetic waves used for the measurements do not weaken them. Snow particles are almost seethrough to the GPR and can thus be disregarded. Some drawback with GPR is that they can be rather expensive, approximately $150,000 SEK[44] for an entry-level kit. The measurements also rely on the dielectric constants of the measured materials. Even for a machine calibrated for snow, this parameter still changes depending on the size of the snow particles and possible ice sheets throughout. The main advantage of a GPR is that the data is reliable as interference from the surroundings is negligible, and the measurements can occur and be processed in near real-time[41]. Furthermore, since the range of the GPR depends on the frequencies it emits, where lower frequencies lead to longer wavelengths and greater ranges, the measurement of snow and ice can occur at great depths since the frequencies needed to penetrate snow and ice are relatively low. The output data, be it A-scans or B-scans, do not directly give the distance but the relative time delay of the waves. Thus, signal processing is needed to get the depth. One proposed solution is to utilize machine learning to derive the distance. This approach has been applied in numerous previous works with good results[45][46].

To conclude, GPR is a robust and reliable sensor, however a bit expensive. The fact that it measures the changes in dielectric properties in materials and, thus, the distance to them is independent of the surrounding environments and not necessarily bound to the ground gives the GPR great potential to measure snow depth in real time.

3.1.6 Final sensor choice

Based on the following criteria:

- Robustness of the sensor
- Positioning precision required to perform measurements
- Possibility to mount on a moving vehicle
- Potential to convert the measurement data in real-time

A final choice of the sensor was made. The SAR is not applicable since it cannot be mounted on a ground vehicle. The premise of SAR is that it increases the apparent size of the aperture by moving large distances above the measured point. LiDAR works optimally when making a 3D model of the surroundings. It cannot, however, penetrate snow. To measure snow depth, the original 3D environment around the measurements needs to be known, thus making LiDAR incapable of taking measurements in real-time at new locations.

Ultrasonic sensors have a similar problem. Ultrasonic is a widely used snow measurement sensor that is cheap and readily available. The primary way ultrasonic sensors are utilized to measure snow depth is by measuring the echo time of no snow and then making measurements again with snow. The shorter the response echoes, the more snow is below the sensor. This is not applicable as this does not work on a moving vehicle where the height of the sensor changes. The sensor standing out after being subjected to these criteria was the GPR because it fulfilled all the requirements. From the literature study, measuring snow depth is possible with

contact with the ground and when placed at a distance above the snow. This is possible due to the functioning of the GPR, measuring changes in dielectric properties, leading to the possibility of dissociating air from snow and snow from subsurface materials. The time of flight between reflections of the signal is calculated to perform the measurement, leading to the acquisition of a depth value. The GPR is also robust enough to use in snowstorms and high winds and mounted on a moving and vibrating machine as the radiowaves are not heavily affected by these environmental parameters.

Finally, the data recorded from the GPR are A-scans and can be combined in real time into B-scans. However, to get depth measurements from underneath the GPR, it is possible only to analyze the A-scans, which have been reportedly done close to real-time. The GPR is, therefore, the main choice for further studies of depth research.

3.2 Acquisition of GPR data

To design methods to extract a depth value from a sensor, the values that can be obtained and the output data type must be analyzed to extract what interests the project. Different methods were considered. Constructing a GPR, finding simulation data or simulating data fitting this project, and acquiring a real GPR to perform specific tests. A GPR is, as stated in paragraph 3.1.5, a pricey sensor, and the ordering of several components were deemed risky before the theory of using GPR as a tool was validated to be fruitful. Simulated data of snow mediums for GPRs was not found, or at least not in a usable format. The choice of simulating own GPR data was made due to the findings of an open-source GPR simulator called gprMax[47].

3.2.1 GprMax

GprMax is an open-source software allowing for the simulation of GPR data by creating scenarios where materials, layers, and their electromagnetic properties are defined. Figure (3.6) presents a simulation of the GPR signals when scanning over homogeneous snow on top of a layer of stone. It stimulates the field strengths in both V/m and A/m in all three spatial directions. The most commonly received signal to look at is the field strength of the voltage, V/m, in the z-direction. The peaks and valleys indicate the received signal; from it, it is possible to determine how the measured substrate is composed. The first peak in each trace is the reflection when the medium changes dielectric properties. In this example, the first peak is the transition from air to snow, and the second is the transition from snow to stone. The deeper the radar waves travel, the weaker the reflection will be; however, if the change in dielectric property is large, the peak will be more defined. These traces are, as mentioned above, called A-scans.

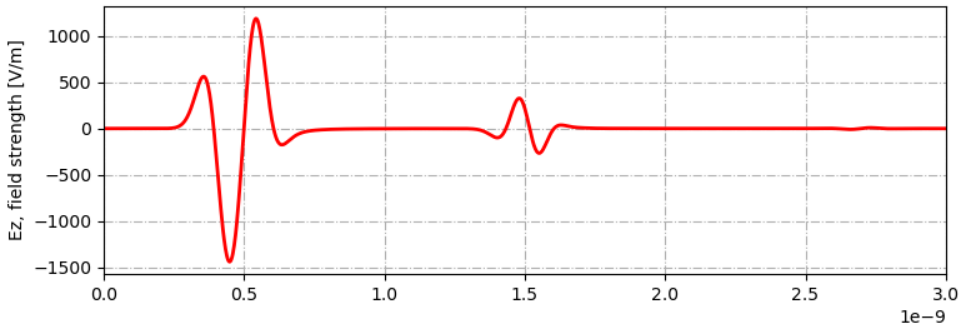

Figure 3.6: Example of a simulated A-scan representing the response to the sent pulse

Combining many A-scans can achieve a 2D scan of the traversed subsurface. The A-scans are rotated 90 degrees in the x- and z-axis. Because of this rotation, a gradient of colour is needed to represent the peaks and valleys of the A-scans. In Figure (4.5), red indicates a peak, and blue indicates a valley. These B-scans are the most commonly used output for data analysis.

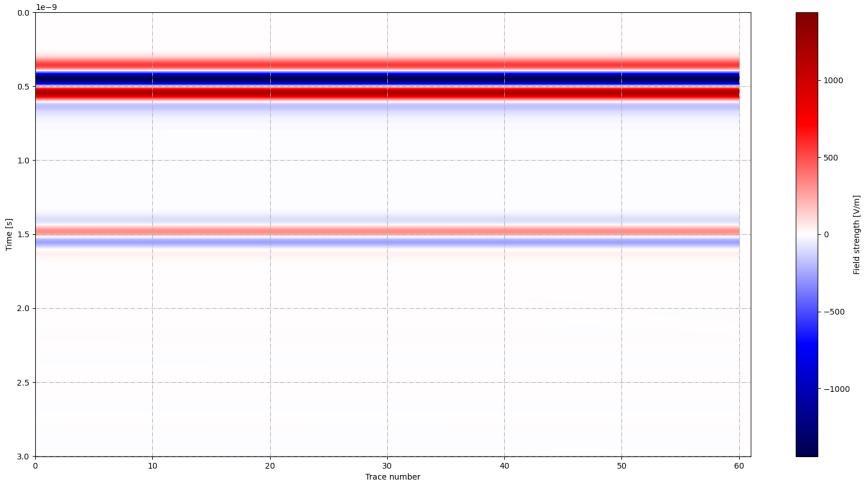

Figure 3.7: B-scan of two layers of differing di-electric properties

GprMax is a program with extensive options from modelling shallow soils to creating complex scenarios where materials have dispersive properties, are heterogeneous, have rough surfaces, etc. The program uses Python and functions by solving Maxwell's equations according to Yee's algorithm with the finite-difference time domain[48].

3.2.2 Shortcommings of GprMax

Whilst GprMax is a convenient tool, it does not offer solutions to every aspect of the project. As mentioned before, GprMax is capable of modelling and simulating heterogeneous materials. However, these materials are pre-defined to be a mixture of soils and not other mediums, such as snow. Since GprMax is a simulation software based on solving finite element approximations, each simulation of a specific scenario produces the same result. Due to the simulations being deterministic, creating a dataset to train a neural network is complicated. There is no way to add noise or irregularities to the simulations; thus, a dataset would contain multiples of the same A-scan. This can be solved by preprocessing the data to add some unique random noise to each signal before using it to train a network. How much noise is added and what type of noise dramatically affects the network's performance is no guarantee that the preprocessed signals resemble actual signals. To avoid these problems, it was deemed necessary to execute real-world tests.

3.2.3 Real-world GPR data acquisition

A series of tests must be conducted to improve and adapt a proposed system for real-world applications. These tests aim to evaluate the system's ability to perform robustly in various scenarios and identify potential problems that may arise outside ideal and simulated conditions.

The first aspect of interest is the system's ability to obtain accurate depth values for different thicknesses of snow layers. Training a network on a dataset with varying depths will be crucial for achieving this goal. At first, simulated datasets will be used, but real-world datasets will represent the desired application better. Another important consideration is the effect of different densities and humidities of snow on the system's performance. These variations wish to be tested to determine the response of the GPR. Further parametrization of the layers may be necessary to account for any significant uncertainties in the ground values. In addition to the snow, it is essential to detect and account for other materials lying in the snow, such as tubes or stones, to prevent incidents. Tests will be conducted to determine the system's ability to detect and accurately measure the depth of these materials. To ensure the accuracy of the results, tests will be conducted at locations where ground truth can be obtained through manual measuring techniques such as a ruler or boring a hole. Multiple samples will be taken for each test at different depths to improve the future network's performance, as more data means better training.

Due to the absence of reliable and significant amounts of snow in the Gothenburg region, finding an alternative location to conduct the tests was necessary. Serneke Skidome, an indoor ski facility that uses artificial snow, was identified as a suitable location. The facility has cooling lines to ensure uniform snow quality, which will be visible on the GPR. A thick snow layer is present inside, making it possible to build or dig tests to reach different depths. The facility was welcoming and eager to help the needs of this project by providing extra snow in the chosen test location. A preliminary visit to Skidome was conducted to assess the feasibility of the tests and determine what preparations would be needed for the next step. The snow in Skidome is made by producing ice cuts and sent out to the facility as

slush. In addition to the controlled conditions in Skidome, this leads to snow with mostly uniform characteristics.

Figure 3.8: Sample of artificial snow from Skidome

As observed in Figure (3.8), the snow in Skidome is granular and dry. It is also hard to pack together, and each grain is quite large. This leads to snow layers with many smaller air pockets, as presented in Section 2.3.

Cooling lines are present under the surface in most places of Skidome, but between the central pillars, there are none. The wish to perform tests over even ground was more substantial than testing against cooling lines; therefore, a testing area between pillars was chosen. As tests and materials had to be prepared, another visit to Skidome was scheduled to prepare the tests.

A general plan was made before the actual testing and building of the test took place, illustrated in Figure (3.9).

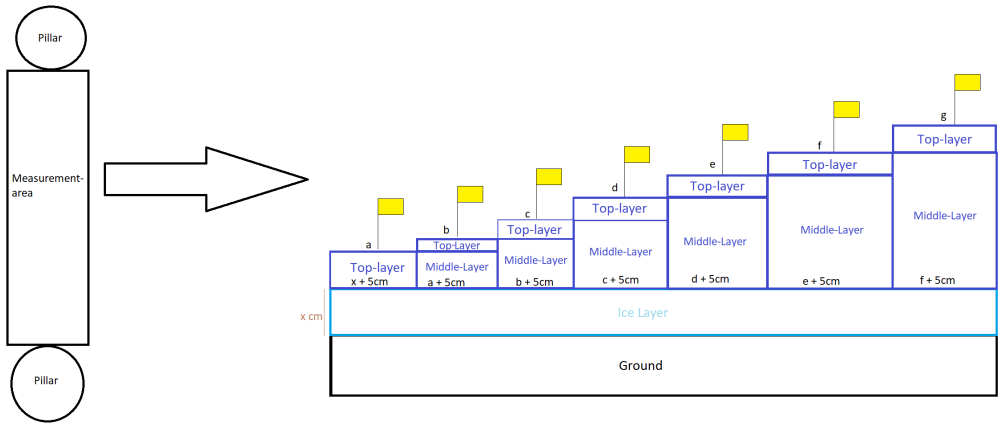

Figure 3.9: Schematic representing the tests to be made in Skidome

Seven tests were built at different depths, with two presenting special conditions, one being a long packed straight line and the second a puck of loose snow over packed snow, to see the difference in response. The creation of tests was successful, but some unaccounted-for complications arose. Building tall tests meant that the one-meter metal ruler could get stuck in the snow and freeze; it also meant more uncertainty as a hard layer of ice could be misinterpreted as the ground, so a limitation on the maximal test height arose. The hardness of the snow layer also imposed a minimal height for testing. Digging a hole to reach shallow depths with the help of a shovel proved too time-consuming and complicated, leading to the minimal testable depth being 46 cm.

Figure 3.10: Reference measurement of a built test at Skidome

Figure (3.10) shows a depth measurement and flagging of the measured depth for better identification when measuring with the GPR; it later proved to be erroneous and has a depth of 600mm, demonstrating the human error factor in such measurements. Having to adapt to the properties of the snow, some changes had to be made to the planned test shown in Figure (3.9) resulting in depth-measurements made at 460mm, 490mm, 600mm, 640mm, 710mm, 900mm and 990mm.

The GPR used for the tests is from Malå, the GX450 operating at a frequency of 450 Mhz as well as a tablet to control it, obtain and observe data. Snow was present in large quantities when performing measurements, so additional tests were performed on natural snow, enabling the possibility of comparing real and artificial snow. Tests were made outside by building a puck measuring 46 cm depth, passing the GPR over it, and pulling it along a flat surface. The MALÅ GPR takes regular scans, each 2.5 cm triggered by the odometry wheel at the back of the GPR as seen in Figure (3.11). This enables the MALÅ software to plot a B-scan with an x-axis in meters.

Figure 3.11: Gathering data with MALÅ GPR at Skidome

While performing the tests, the depth values could be obtained from the control tablet included with the GPR. This led to the need to calibrate the measured depth compared to the real depth. A speed of $125 \frac{\mathrm{m}}{\mu\ \mathrm{s}}$ was used to extract the correct depth value.

Tests were then performed inside Skidome. The difference between the GPR's measurement and the reference depth was noticed starting with the shallowest test.

This led to another calibration of the GPR at a speed of $134\frac{\mathrm{m}}{\mu\,\mathrm{s}}$, meaning that the artificial snow absorbed less energy than the natural snow outside. An additional test was performed after the planned tests: pulling the GPR along a longer track to analyse how the cooling pipes' response looked. To ensure the quality and precision of the measurement, several measurements were realised at each test floor.

3.3 Processing of GPR data

With the data collected, some processing of it was necessary for later implementation. This processing was different for simulated and real-world data.

3.3.1 GPRMax

The data obtained from GPRMax in Section 3.2.1 does not provide a depth value. It, therefore, needs to be transformed and analysed. Post-processing is needed to transform the data into a usable format. The A-scan or pulse response can be transformed into a vector that is easier to obtain information from. Usually, the pulse response from a GPR needs to be interpreted by software or a user to convert the output from the GPR to actual depth measurements or indications. Experienced technicians can do this manually. However, this can be a tedious process with some uncertainty as wave propagation speed is not always displayed, as seen in Figure (3.6) compared to Figure (3.13).

There is, as such, an interest in automating the process of depth obtention through vectors representing the A-scans. One means to achieve this would be to import the vector into a neural network. Said neural network would train on A-scans with a known depth and learn the characteristics of each scan and what depth they correspond to. Such a network could, after training, be used to classify the depth of new A-scans. A neural network needs a dataset to train on, and the A-scans in this training set should be as unique as possible to train a confident and robust network. The A-scans from GPRMax are numerically calculated without stochastic deviations such as noise. The traces for a specific depth will all be numerically identical. To create a unique dataset for the network to train on, some processing of the GPRMax A-scans is needed. Introducing a small noise to each trace makes them unique enough for the network to consider it being new traces. This would not be needed for real-world A-scans as these are already unique.

3.3.2 Physical data

The GPRs from Malå, used to obtain the physical test data, save data in special formats called rd3 and rd7, depending on the bit size of the measurements. Those could be extracted from the radar by plugging the connected tablet into a computer and sending it to email. It was possible to visualise this data using Malå's website and the Vision software. The problem was that GPS data had to exist, which was not true for the tests made inside Skidome. A solution was found in RGPR[49], an open-source software developed in R for the visualisation of GPR data. The

program is straightforward; it takes in the files with their headers and calibrated propagation speed, allowing visualisation and primary processing.

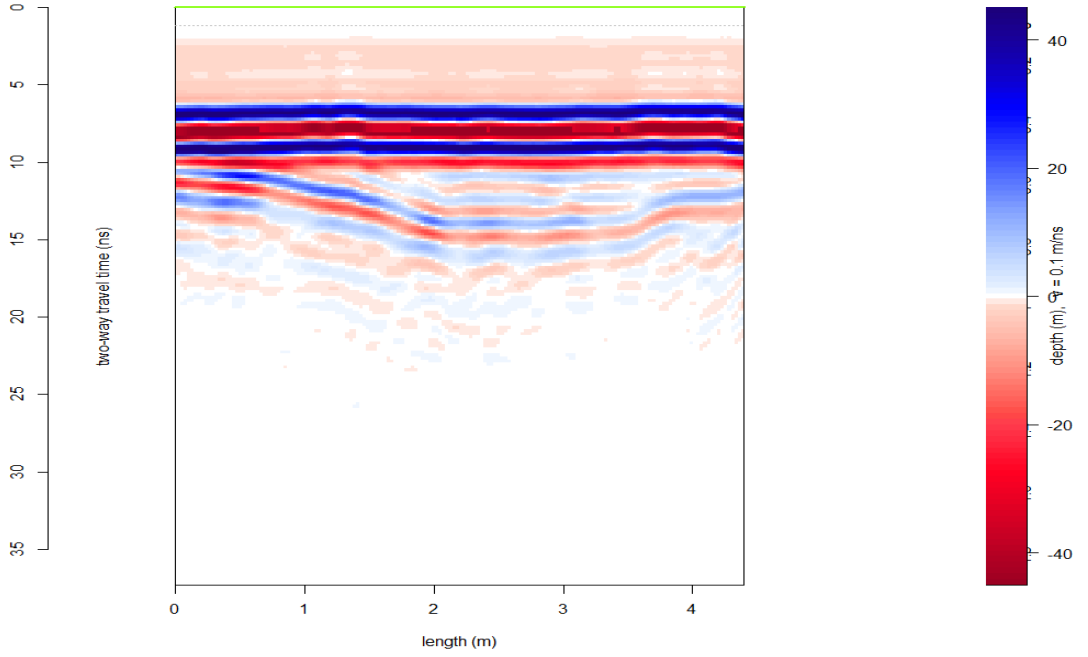

Figure 3.12: B-scan generated with RGPR representing the snowstair at 710 mm

Above, in Figure (3.12), a B-scan from one of the tests made inside Skidome is observable. To the left, the response-time axis indicates the time the two-way travel time of the wave when it reaches that point in the medium. On the right, the waves' velocity and the extracted depth can be read, and the length over which the measurement was made is visible at the bottom. It is worth noting that a depth value is given through the calibrated velocity of the GPR at the moment of the measure, which can be erroneous. This is the simplest way of presenting each measurement of the GPR. Observing the Figure (3.12) makes it possible to see the performed test. In the beginning, the GPR is dragged along a flat section of snow and at approximately one meter, it begins to escalate the stair test observable from the point at $(1, 10)$. When the GPR is on top of the test area, the response becomes flat again; this is the part of interest where the depth has to be guessed. The image shows the opposite of the stair shape as it always recognises the GPR as a height zero.

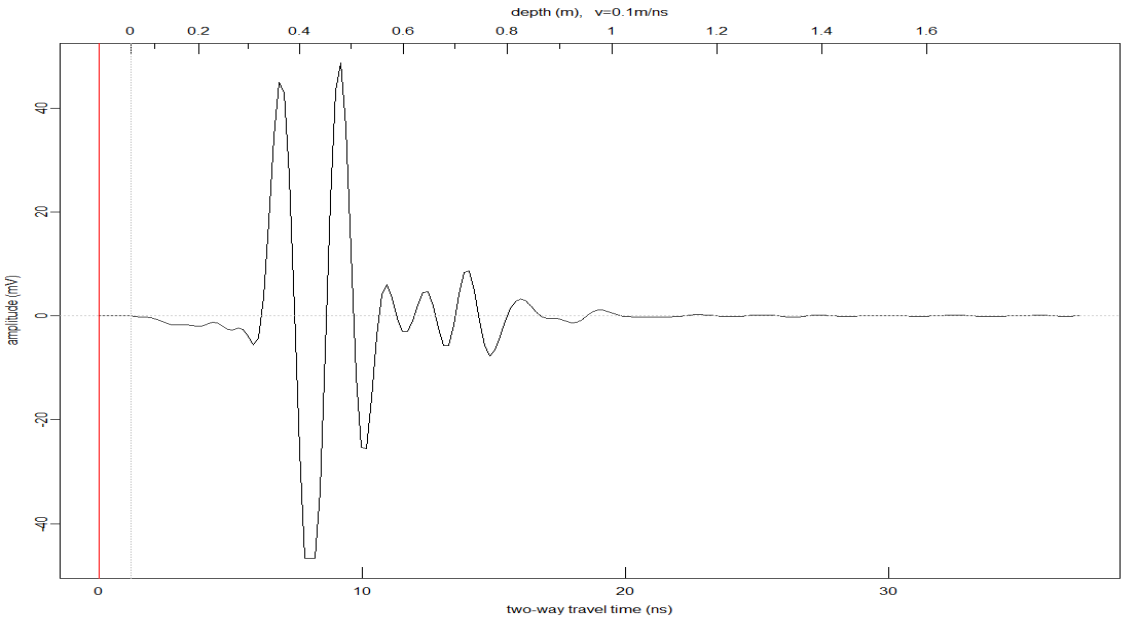

Figure 3.13: A-scan generated with RGPR representing trace 100 in Figure (3.12)

From the B-scan in Figure (3.12), it is possible to extract the traces (A-scans) by simply choosing which trace one wishes to visualize. Here trace 100 corresponds to the moment the GPR was on the stair. The appropriate response time is between the first prominent peak at t=8ns and the peak at t=14ns. This data can then be fed to a network for training, utilising the vectors representing the GPR on top of the test stair.

Instead, a proposed solution is to utilize a neural network to train the pulse responses to classify the depth. A neural network will be trained to process the vectors graphically, looking at features indicative of the reflections against different materials. The network can be trained against ground truth labels to predict the depth of a given A-scan. Therefore, a training and validation set is created along with the simulations made in gprMax. Later, the data from RGPR was separated with the same method.

Credible simulation scenarios in GPRmax were developed by studying the electromagnetic properties of snow. A model of snow layers with different properties was devised, from loosely packed to densely packed snow. An increasing depth level is also considered to train the network. The interval is made to go from 10 cm to a meter since deeper snow doesn't have an incidence in this study. The difference between the models will be the distance between the first reflection and the second, as shown in Figure (3.6).

Other tests to see the cooling pipes were made. The B-scan resulting from the abovementioned measurements is shown in Figure (3.14).

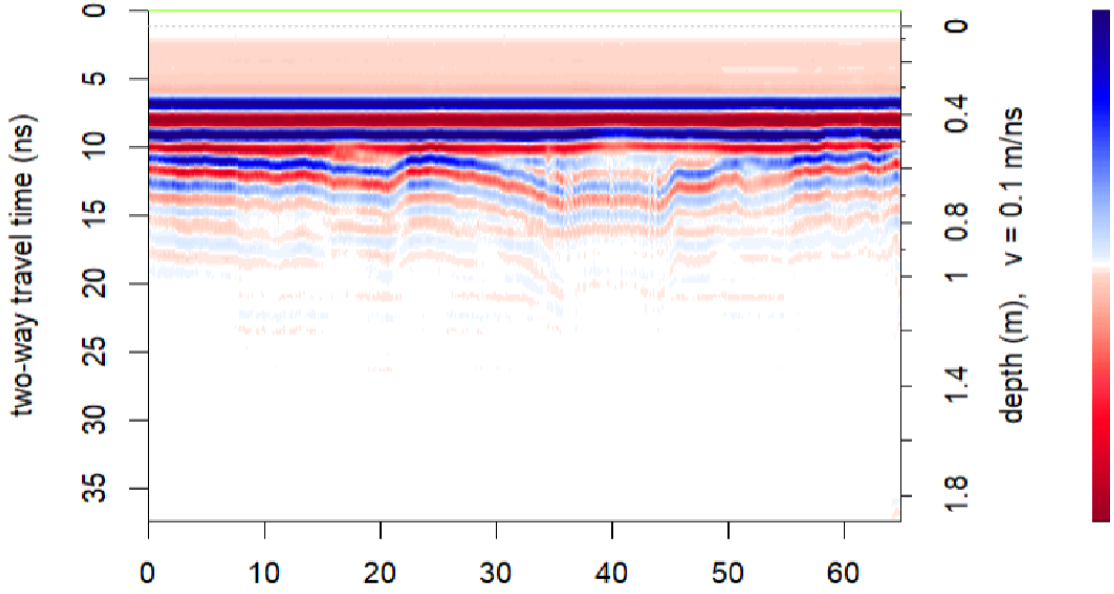

Figure 3.14: B-scan over cooling pipes generated in RGPR

The pipes are clearly noticeable from index 35 to 45 on the x-axis. Obtaining depth can be done by analyzing the shape of the parabola trough function in RGPR.

3.3.3 Neural network structure

As the output from the GPR scans is 1-dimensional, see Figure (3.6), the neural network processing these signals needs to consider this. One solution would be to use a fully connected or dense network, proposed in Figure (3.15). These networks take each value of the 1-dimensional input vector and learn how these values individually correspond to the final depth. It can find the positions where the signal is greater and learn that these are the depths that the GPR has found layers in the subsurface. These networks usually need to train for a long time since many parameters can be trained when everything is fully connected. It is also susceptible to noise as there is no correlation between neighbouring vector values according to the network.

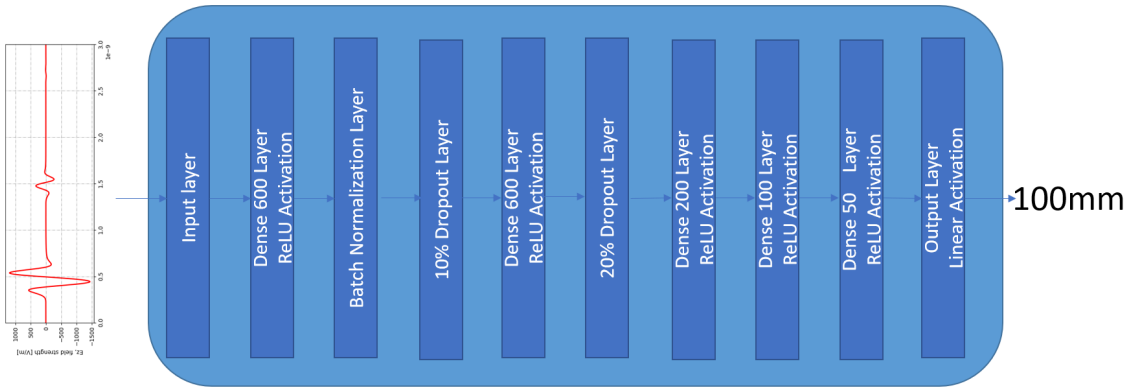

Figure 3.15: Proposed dense neural network structure

Another proposed solution is to utilise 1-dimensional convolutional layers with a fully connected layer at the end, proposed in Figure (3.16). These networks instead apply a sliding convolution to the input. The result from one convolutional layer can be interpreted as a feature map of the information instead of each value being considered. It can learn how the pulse response for air-snow and snow-ground look and what characteristics they hold. In doing this, the network will learn a more general way of predicting the depth. The convolutional network is not as susceptible to noise as it will look for features of the input vector and not the individual values. To create a classification of these features, the last layers consist of fully connected layers that interpret what features correspond to what depth. These networks have fewer parameters to train and can thus be made more complicated while training more quickly.

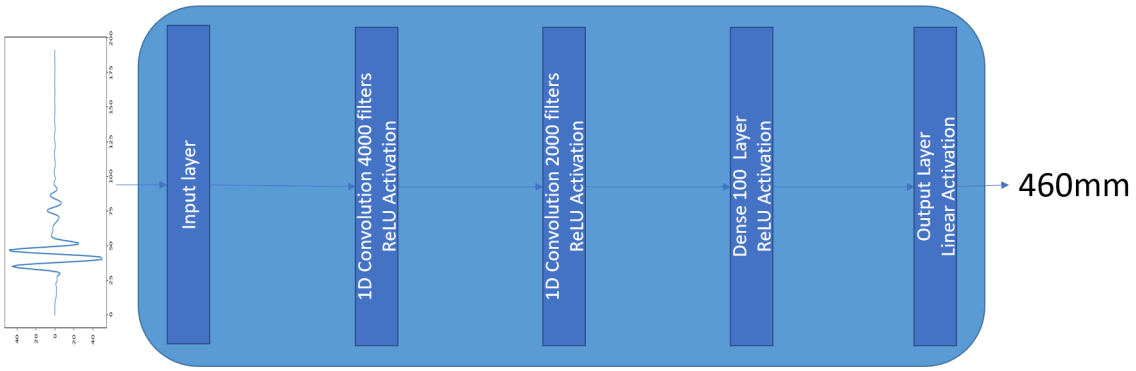

Figure 3.16: Proposed convolutional neural network structure

There are mainly two factors that are considered when creating and training a neural network. The network must be complex enough to train and converge to a solution. This is achieved by including enough layers with large enough dimensions for the network to learn. However, including too many layers can and most often will lead to the model overfitting to the training set. To avoid this, layers are removed or shrunk to force the network to develop a more general structure. Implementations of particular layers, such as dropout layers, also help to mitigate overfitting. Both models utilise the mean square error loss function since the labels are strictly numerical.

3.4 Construction of a Cost-Effective Self-Assembled Ground-Penetrating Radar

After successfully acquiring real-world data using the tested frequency and GPR, and with enough time left before the final deadline, there is a desire to experiment with a cost-effective self-assembled ground penetrating radar, henceforth C.E.S.A.-GPR, designed explicitly for shallower measurements. The purpose of this section of the thesis is to deepen the knowledge surrounding GPR technology as well as experiment with different frequencies. This is done by designing a GPR with a higher frequency than the one used for the previous tests. All this for a low budget. A design was

found, made by Mirel Paun and posted on Hackaday.io[50]. The proposed design mainly consists of the following:

- Arduino Mega 2560
- LCD Screen
- An Oscillator: JTOS-850VW+
- An RF attenuator: PAT-10+
- A low noise amplifier: PSA4-5043+
- A bias tee: TCBT-14+
- A splitter-combiner: ADP-2-4
- A mixer: ADE-2ASK
- 2 PCB boards designed by him
- Conductors, resistances, and connectors.
- An antenna

The oscillator works in a frequency range from 400 to 850 mHz, and the overall design is that of an ultra-wideband GPR. The total cost for the radar components was: 4797 SEK. The prototype aimed to be built will slightly modify the original design using a different Arduino and antenna. For this antenna, the plan is inspired by the reference but with some changes, and the box's design is matched to products found locally, as well as the size of the antenna. Using an existing project was deemed the best solution due to the lack of microelectronics and radar design knowledge. The schematics for the PCBs are shown in Appendix A.1

3.4.1 Antenna choice and design

As presented in the theory section 2.2.2, the antenna's parameters will allow for tuning of the frequency and performance of the radar. An antenna matching the desired project was, therefore, designed. The oscillator of the chosen design works from 400 to 850 MHz. The recommended type of antenna was an antipodal Vivaldi antenna built from PCB material. The Matlab toolbox was used to design the antenna since it can model all the parameters for its shape and simulate the frequency and spread pattern of the radar wave[51]. Articles were read to get a better idea of a starting model of a Vivaldi antenna as well as recommendations from the comment section of the radar project[52][53]. The internet user designed the antenna with dimensions 12x13x2 cm and used double-sided PCB as material. It presents a bandwidth from 250 MHz to 1000 MHz with a mean realised gain of 17 dB presented in Figure (3.17)[52].

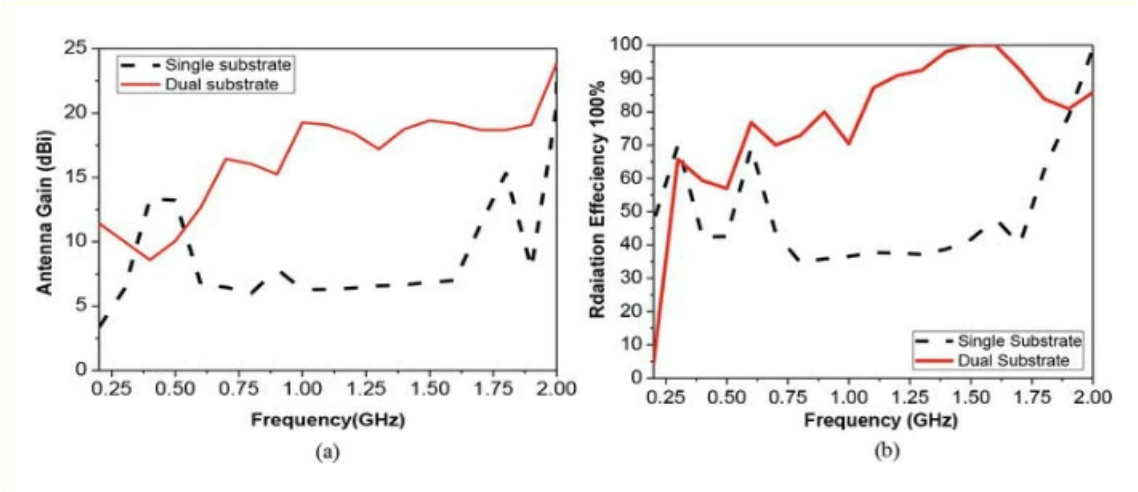

Figure 3.17: Antenna gain and realised gain for the proposed antenna

The material chosen to build the antenna is important but must be available relatively quickly. FR4 PCB material was ordered since it was readily available cheaply. The properties of the PCB material received are: are:

Width	Length	Thickness	Dielectric strength	Relative Permittivity
20 cm	32 cm	1.67 cm	20 MV/m	4.4 A

Table 3.1: Properties of the double-sided PCB made from FR4

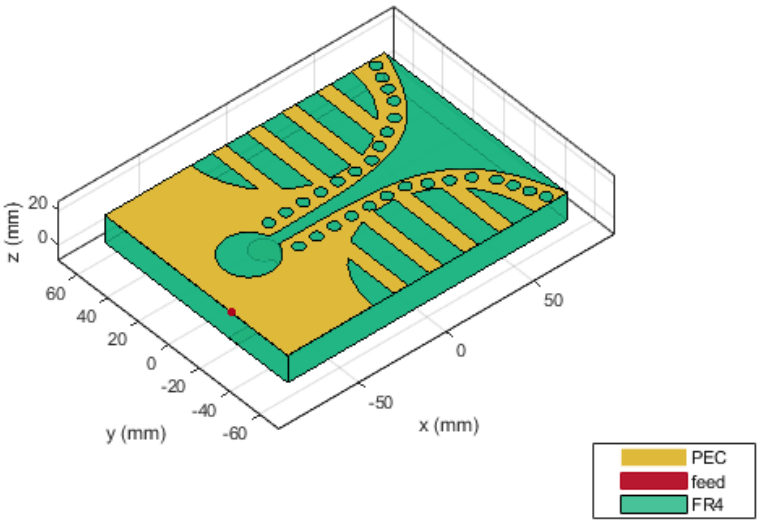

Figure 3.18: Antenna stack with dielectric layer modelled in matlab

Other views on the antenna stack are presented in Appendix A.2. Then the realised gain was computed. Matlab does not have an extensive library of dielectric materials leading to the values being approximative. The corresponding gain and realised gain are shown below:

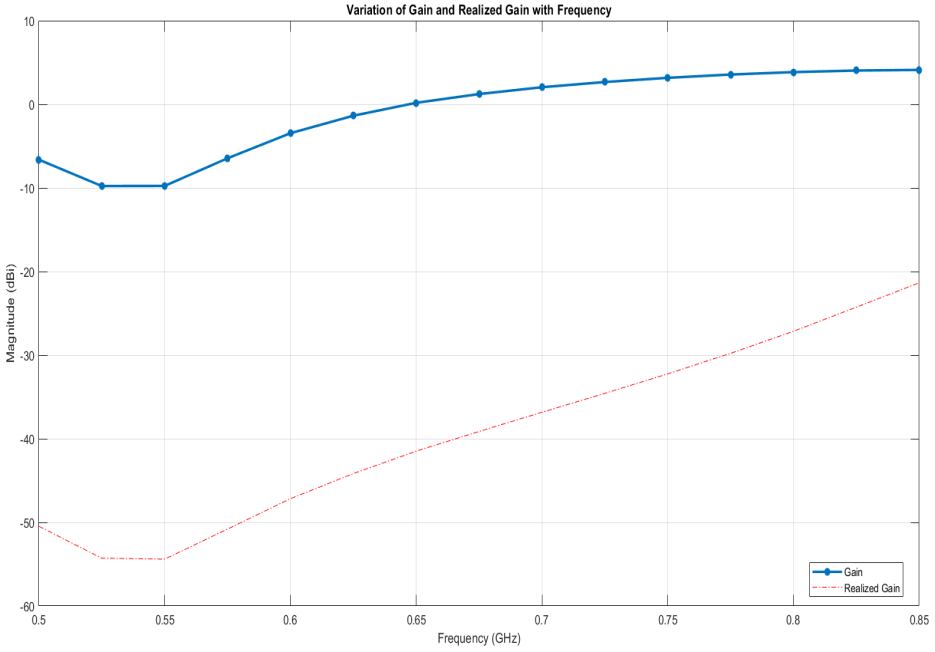

Figure 3.19: Gain and realised gain of the designed antenna calculated in matlab

The positive gain after 650 MHz is positive for testing the efficiency of a higher-frequency radar. Differences between Figure(3.19) and Figure (3.17) are noticeable as the gain is smaller in the simulated scenario than from the reference. This is acceptable as human error due to the lack of knowledge regarding antenna design. The radiation pattern of the antenna showing the directivity of the transmitted waves is then:

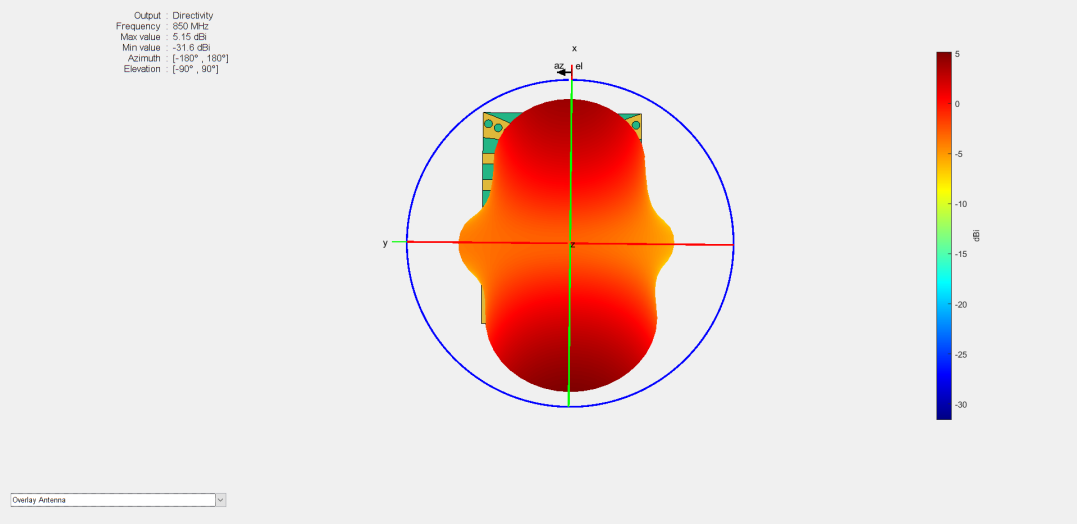

Figure 3.20: Radiation pattern of the antenna with an overlay generated by matlab

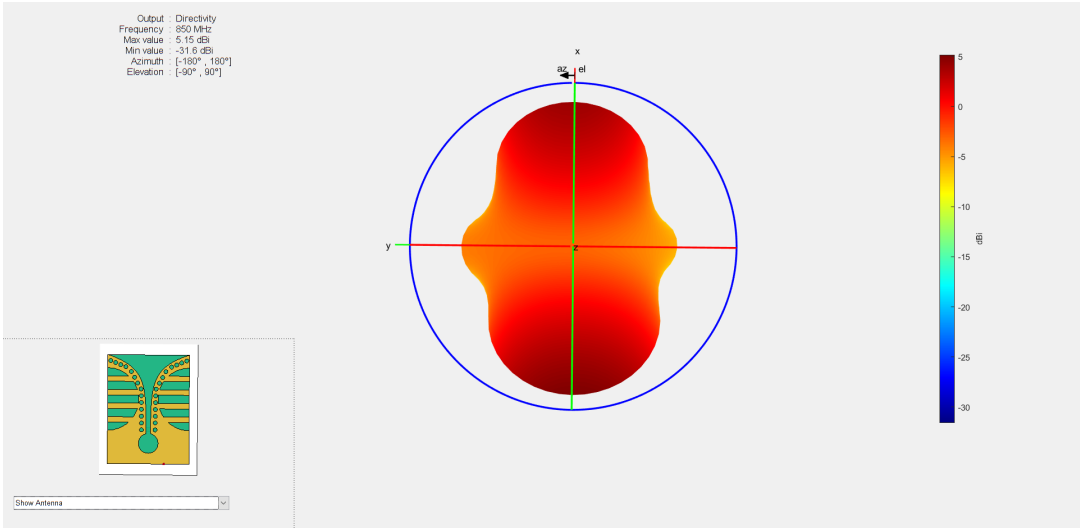

Figure 3.21: Radiation pattern of the antenna without overlay generated by matlab

The above-presented Figures (3.20) and (3.21) show that the designed antenna is directional with a high gain in the vertical direction. This is the desired result, as the antenna will be directed towards the ground. The effect of backward radiation has not been researched.

3.4.2 Construction of the radar

A plastic box with 30 cm height was bought to fit the radar, four wheels, a circular stick to fasten the wheels on, a bumper to trigger the pulses, and a lid to fasten the screen. The Arduino, PCBS, and screen were stacked with pin connectors and mounted on the lid where a suitable hole was cut out.

Next, the antenna had to be built from the FR4 substrate. To do that, the copper had to be removed in the shape of the antenna. A chemical named sodium persulfate was used to do that. From the antenna shape modelled in Figure 3.18, a cover with the corresponding shape was printed to be fastened onto the copper to protect the necessary parts. The non-covered copper was exposed to a chemical reaction to remove it.

3.4.3 Testing of the prototype

This experiment aims to gauge the performance of this home-built GPR against the previous tests. Therefore will, tests of similar nature be performed. The GPR can save the measurement data on an SD card that will be put inside a computer to read and predict the vectors like before.

4

Results

4.1 Simulation results

To evaluate the neural network model and the underlying snow-measuring properties of a GPR, A-scan results were acquired using gprMax. Sixty-five scenarios with a snow layer on top of a ground/rock were fed into gprMax, resulting in the following indicative A-scans.

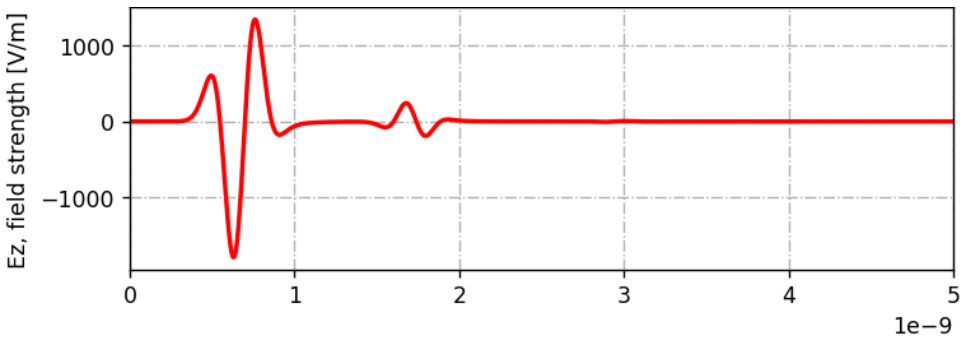

Responce time [s]

Figure 4.1: A-scan: 10 cm snow on top of a ground layer simulated in GPRMax

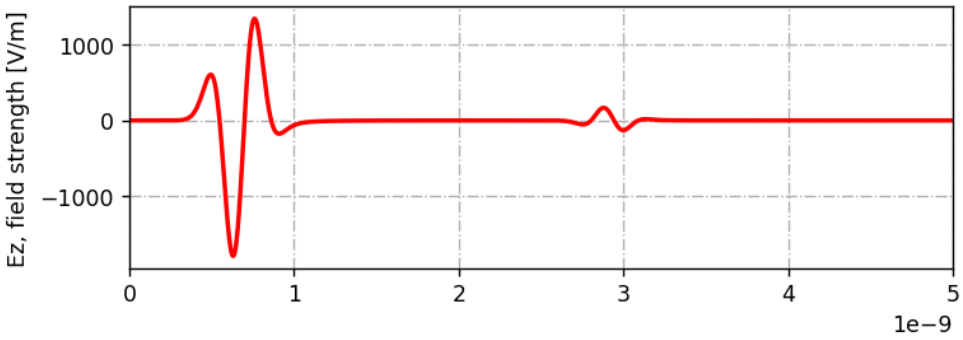

Responce time [s]

Figure 4.2: A-scan: 20 cm snow on top of a ground layer simulated in GPRMax

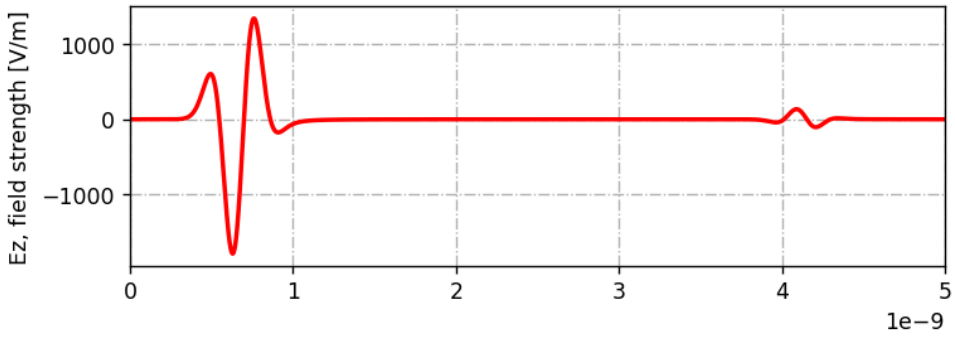

Figure 4.3: A-scan: 30 cm snow on top of a ground layer simulated in GPRMax

From the A-scans provided above, it is clear that the strength of the second radio echo decreases as the snow layer deepens. Additionally, the time delay between the first and second echo increases in direct correlation with the depth of the snow.

A B-scan was conducted to gain a deeper understanding of GprMax's properties. This involved analyzing a scenario where a metal pipe was buried in the dirt on top of a stone substrate. A Perfectly Matched Layer, henceforth PML, is created around the border to contain the radar waves to the scenario and enable finite element calculation shown below in Figure (4.4)[47].

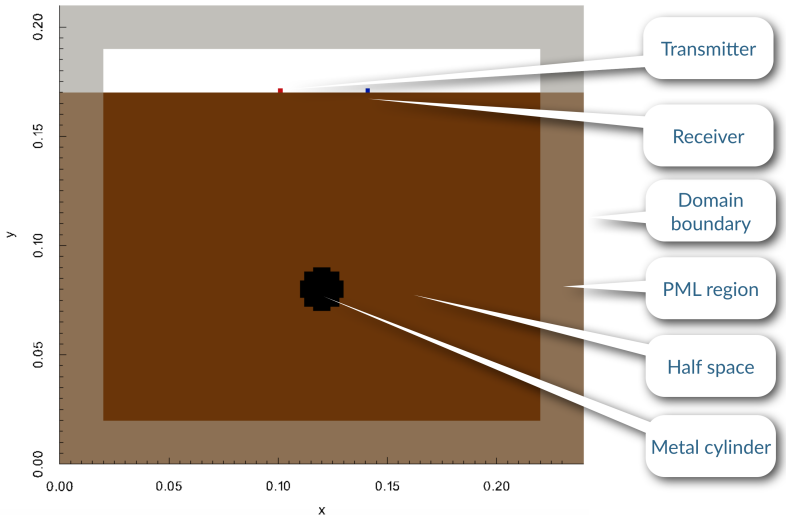

Figure 4.4: Scenario of a metal cylinder buried in a soil substrate simulated in GPRMax

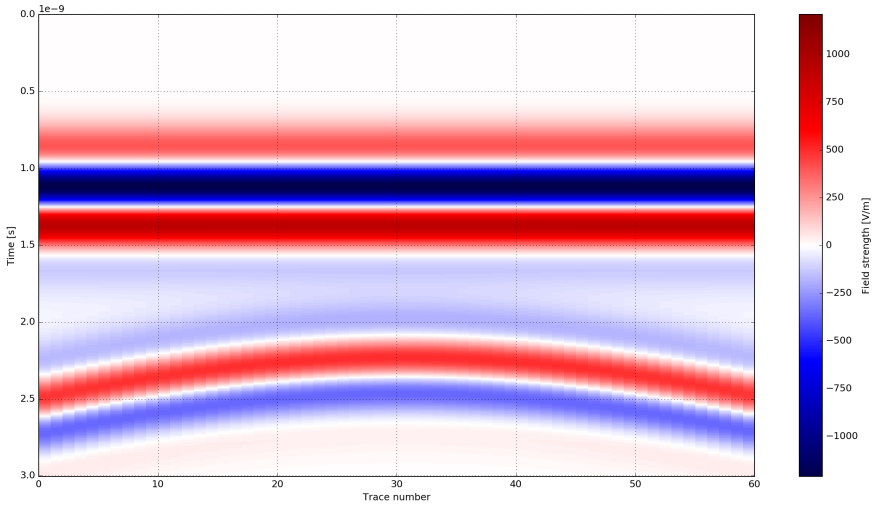

Figure 4.5: B-scan: Metal cylinder buried in a soil substrate simulated in GPRMax

From the resulting B-scan, it can be evaluated that GprMax handles buried objects as predicted in theory by giving a parabolic response to a buried round object.

4.2 Physical testing results

As presented in section 3.3, vectors were acquired from the pulse responses through RPGR, and the network was trained with them.

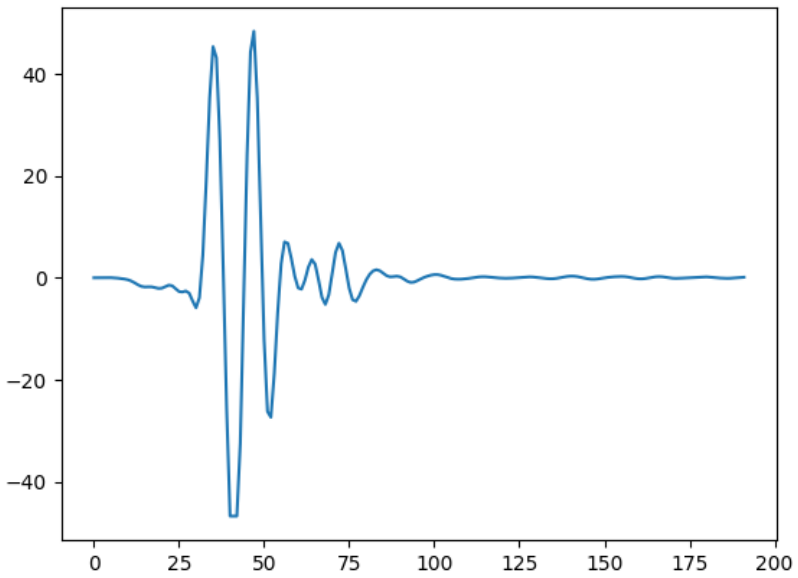

Figure 4.6: A-scan after processing in the neural network

A validation set was then put into the network, and its values were predicted.

The following equation calculates the average error, $e_{average}$.

$$e_{average} = \frac{\sum_{i=1}^{n} |\hat{y}_i - y_i|}{n} \tag{4.1}$$

Where n is the number of A-scans used to train or validate with, $\hat{y}_i$ is the predicted depth for each A-scan, and y_i is the true depth of those A-scans. The average error observed by the network varies each time so over three different rounds, the following errors were acquired.

$e_{average}$	Training set	Validation set
$e_{average1}$[mm]	5.754	8.880
$e_{average1}$[mm]	6.077	8.903
$e_{average1}$[mm]	7.587	10.689

Table 4.1: Average prediction error for three runs of the proposed neural network

The average error for the training set was 7mm; for the validation data, it was 9.5mm.

The tests were performed in a controlled and ideal environment; therefore, the results are better than what could be expected in reality. The values can be determined to be within 1 cm of actual depth values. These results are better than expected at first, especially without other parameters influencing the results, like a first approximation of the type of snow or how much the speed would vary in the snow. The lowest values acquired were 8.87mm of average error in the guesses.

The restricted amount of time with the GPR made the time allotted to perform tests on real snow very short. The amount of data regarding real-world snow was low, making it hard to train a network on it. It is possible to test validation data on it, but that leads to a more significant error than with the validation data suited to the trained network. No actual results concerning the adaption of the GPR to multiple layers of different snow will be presented because of that. An interesting observation is that 9 m/µs separates the real snow from the artificial snow.

Regarding the detection of cooling pipes in Skidome and the measurement of their depth, the following results were achieved through RGPR's hyperbola fitting functions:

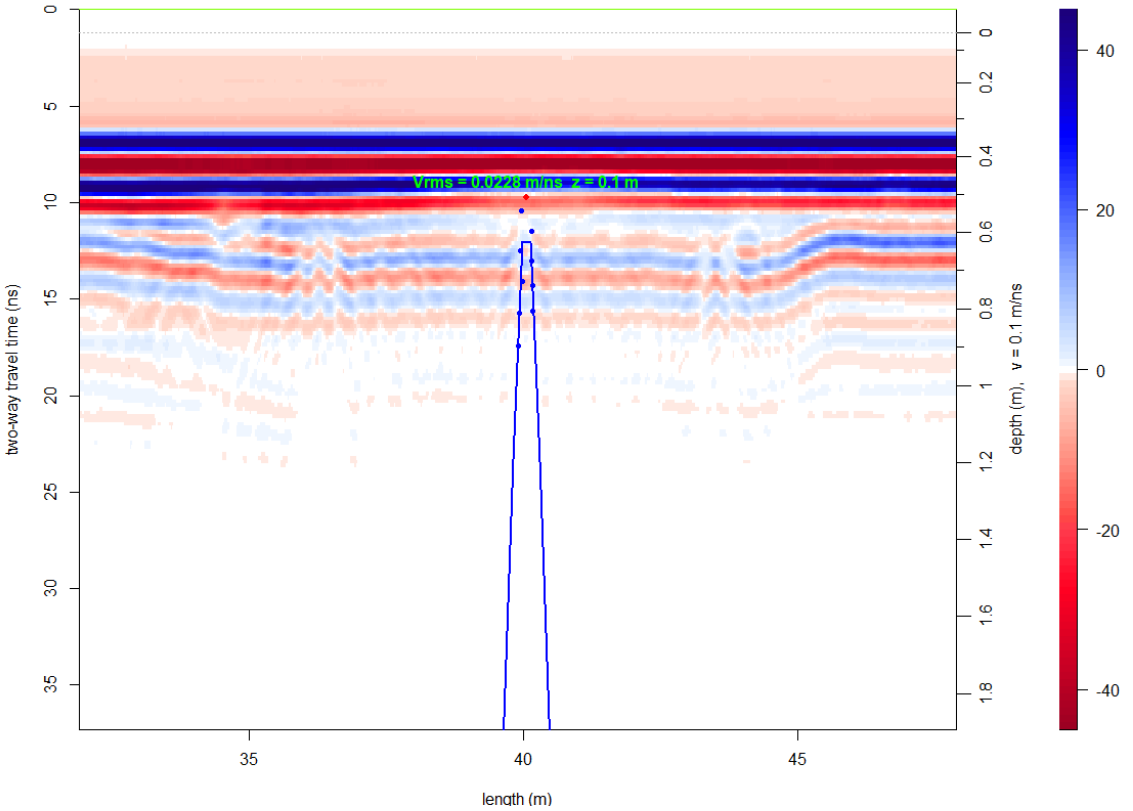

Figure 4.7: Hyperbola fitting of cooling pipes in Skidome generated by RGPR

The location of the cooling pipe in Figure (4.7) is indicated by the red dot at 40 meters on the x-axis. By reading the y-axis, it is observable that it is situated at 10 ns two-way travel time corresponding to a depth of 50 cm. The shape of the hyperbola indicates the thickness of the pipe. It is 10 cm. The malå software could automatically detect and fit hyperbolas after measurements. At the same time, RGPR does it through a manual selection of points to define the hyperbola, so the values are prone to human error and uncertainty.

It is interesting to compare the shape of the A-scan when taken over a cooling pipe to compare it with previous A-scans:

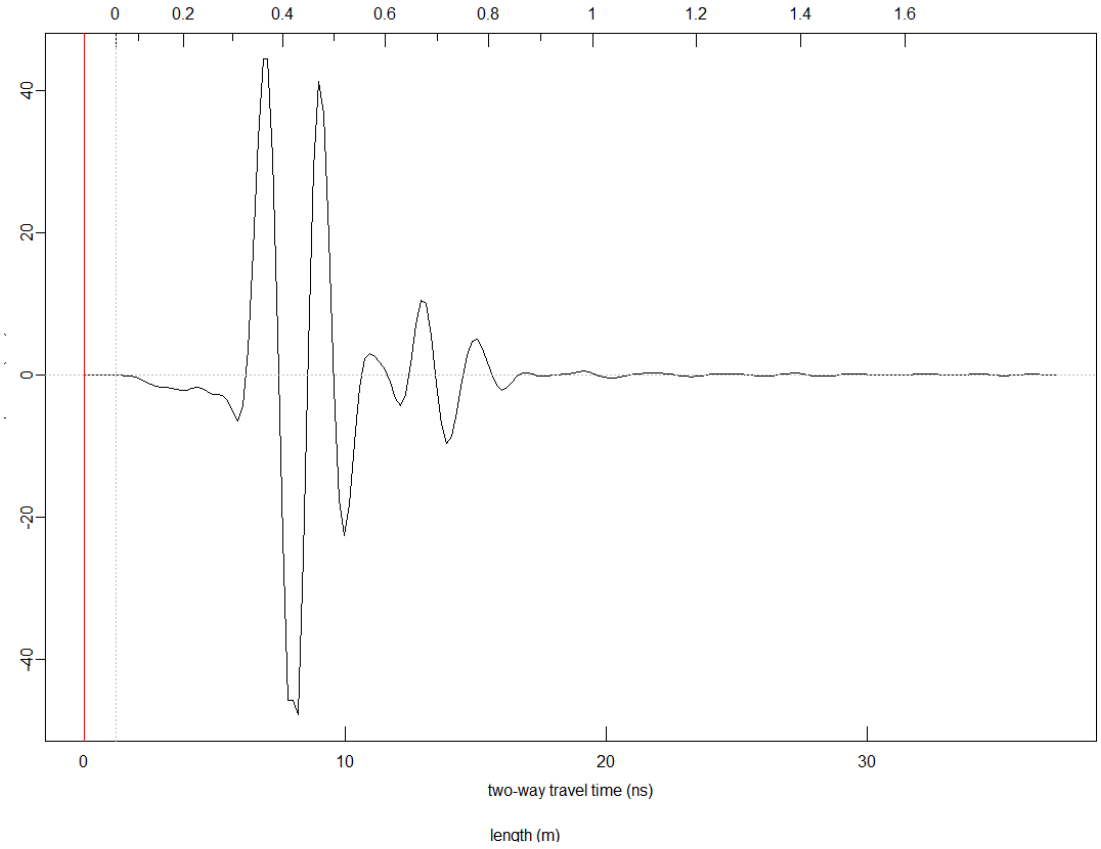

Figure 4.8: A-scan over a cooling pipe modelled in RGPR

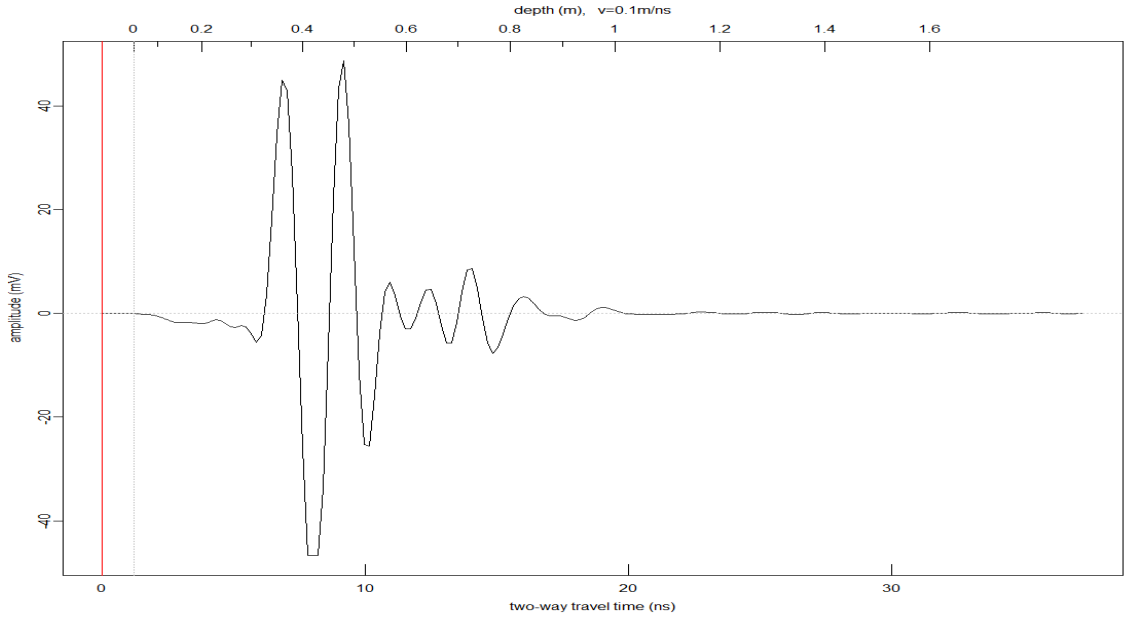

Figure 4.9: A-scan RGPR modelled in RGPR

By comparing Figure (4.8) with Figure (4.9), slight differences are noticeable, but they remain in the scope of other A-scans. This means that pipes and similar

obstacles will not pose problems for the network to provide a depth value. However, this indicates that the network cannot detect cooling pipes only using A-scans of the measurements.

4.3 Proof of concept

Two proofs of concept, henceforth PoC, were made with different ways of collecting GPR data. One used the simulated data to validate the approach's viability. The second proof of concept used real-world data collected at Skidome. The latter is validated to confirm that the concept works in the real world and how it differs from ideal A-scans in the simulated data.

4.3.1 Proof of concept with simulated data

Before training a neural network on GPRMax A-scans, some signals were preprocessed. As mentioned, GPRMax simulates the radio wave propagation and echoes using finite element calculations. The medium the waves travel through is also homogeneous, resulting in the same simulated A-scan for the same depth in each simulation. Training a network on such data would result in overfitting as it could map each type of scan to a depth and not be able to predict new, unseen depths accurately. To counteract this problem, a slight, unique noise was added to each signal that gives every A-scan different numerical values while still carrying the characteristics of snow depth. 6400 A-scans were preprocessed and used to train the network. After training the network on the devised data from GPRMax, the performance can be validated by considering the true and predicted depths by the ANN.

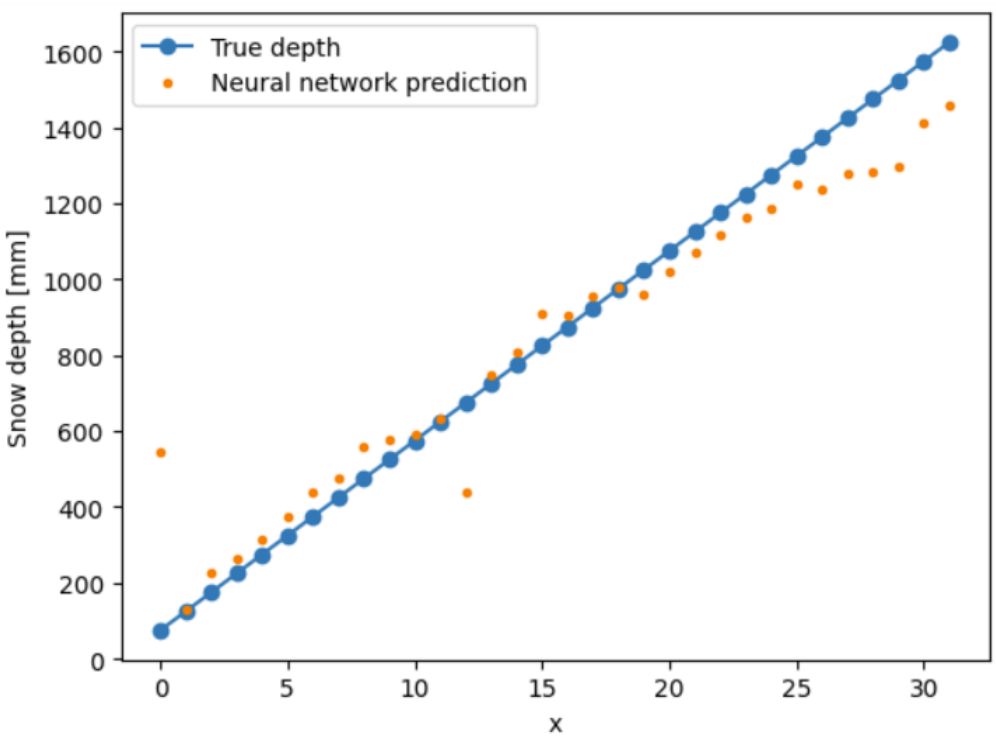

Figure 4.10: True depths plotted against ANN predicted depths on a validation dataset simulated by GPRmax.

The Figure displayed in (4.10) indicates that the network tends to misclassify the deeper snow levels. This could be due to the network assuming an average depth in the middle and making conservative predictions by underestimating the actual depth. The ANN manages to predict the snow depth from validation A-scans with an average accuracy of 5 cm, showing that this solution applies to simulated GPR data; the remaining question was to test it on actual GPR data.

4.3.2 Proof of concept with real-world data

As the PoC for simulated data gave good results, a PoC for real-world data was created. The structure is much the same as for the simulated data. However, there were fewer A-scans to train on this time, namely 447 unique A-scans, as a scan is taken each 2.6cm. Thus, to acquire the same amount of traces as in the simulated case, 166,4 meters of test surface would need to be measured and annotated. In the same way, as for the previous PoC, the model was validated by considering the predictions of the validation set on the trained network.

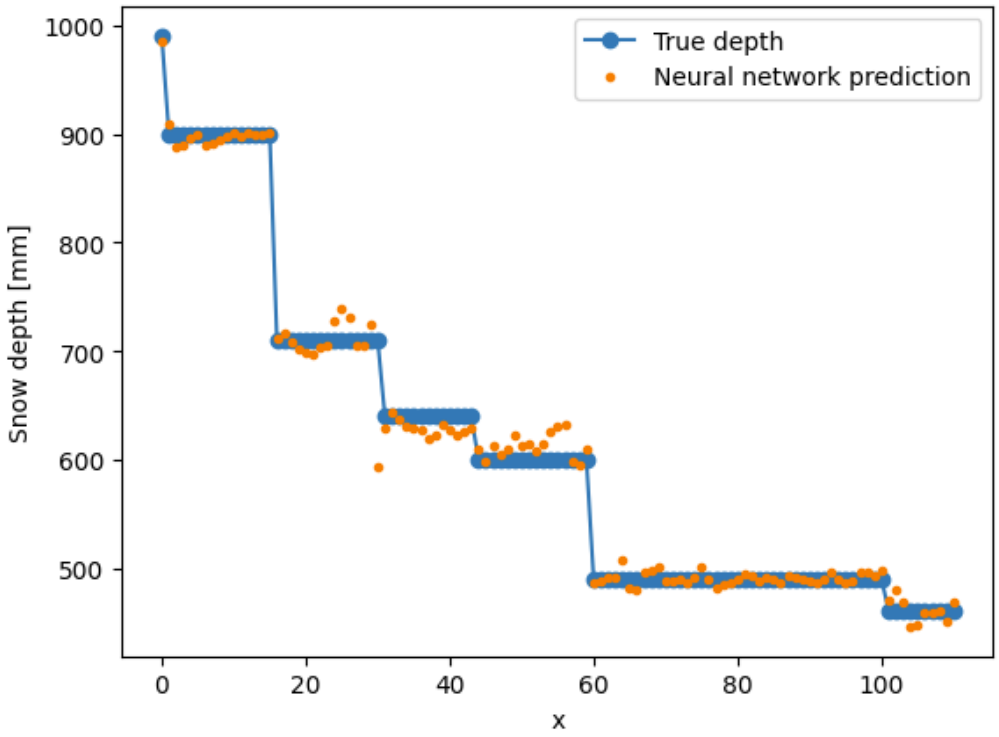

Figure 4.11: True depths plotted against ANN predicted depths on a dataset collected at Skidome with a 450 MHz GPR

Even with fewer A-scans, the model predicted the depth within 1 cm of the actual depth. Some of the variations for each depth can be explained by the variation in height for each measured depth. The actual depth is an average value as the substraight is uncertain and only measured manually with a snow probe, an example of this can be seen in Figure (3.12).

The frequency with which the trained network could predict A-scans is examined. To classify a solution as real-time in this scenario, the frequency must be at least 10 Hz. This is based on the frequency of the current solutions and is needed to see the depth directly under the sensor. Classifying single A-scans, as would be when applied, the neural network took 50 ms, giving a frequency of 20 Hz, ensuring a margin over the requirement.

4.4 Evaluation of C.E.S.A.-GPR

The construction of the C.E.S.A.-GPR resulted in unaccounted-for issues. Soldering the LF- and RF-boards was fastidious and time-consuming, leading to mistakes during the realisation. Components were not soldered as they should have, leading to short circuits on the RF-board. The damaged components were replaced, and the design was tested again. The system then presented issues when using the software responsible for making measurements. It was not possible to access the measurement menu. The error was identified to be caused by the absence of communication between the digital and analogue components of the radar. The exact cause be-

hind this problem was not identified but could be caused by the digital-to-analogue converter MCP4725 or an error in the Arduino's communication busses.

Figure 4.12: C.E.S.A.-GPR PCB control unit

Measurements could, therefore, not be performed, leading to the impossibility of judging the performance of the C.E.S.A.-GPR against Malå's. This experiment indicates that constructing a GPR relies on accurate work and design, especially when the desired cost is to be kept at a minimum. Finally, C.E.S.A.-GPR is presented in Figure (4.13).

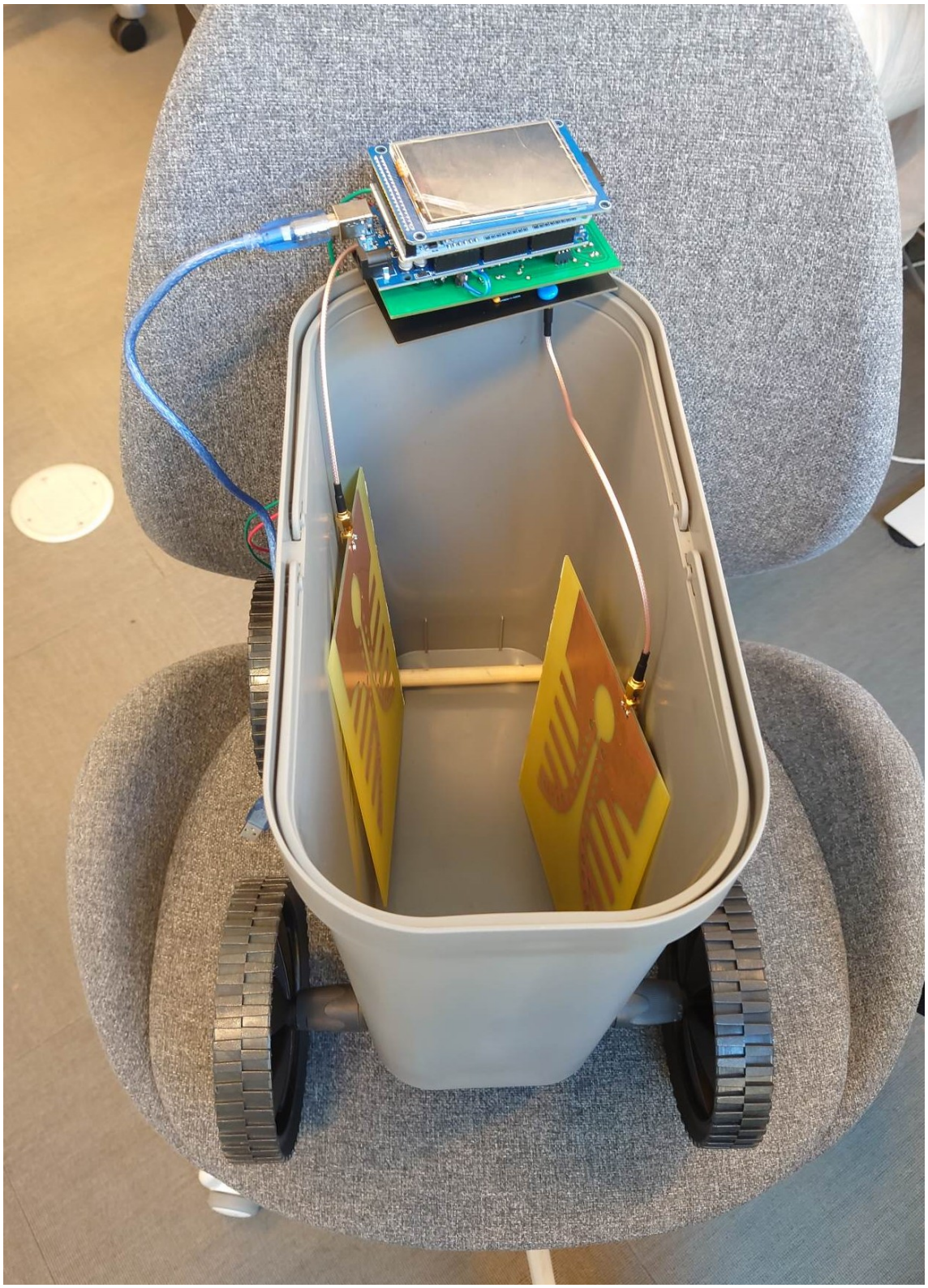

Figure 4.13: C.E.S.A.-GPR

5

Discussion

5.1 Training comparison of simulated results and physical results

As observed in section 4.3, the validation results were better for the real-world data than the simulated A-scans; by observing Figures (4.1) and (4.6), it is possible to see these differences. The A-scans resulting from the simulated data are very similar and simple. There is a first pulse response and a second pulse with similar amplitude and shape. One can observe more individuality by looking at the A-scans from real-world results. The amplitude of the pulses, the shapes and the space between them vary.

The differences in accuracy between these two networks are somewhat attributed to the shorter span of depths, spanning from 490mm to 990mm, compared to the simulated data, spanning from 100mm to 1650mm. The error values can be normalised to account for this difference in depths:

$$990\text{mm} - 490\text{mm} = 500\text{mm} \Rightarrow e_{real} = \frac{10\text{mm}}{500\text{mm}} = 2\% \tag{5.1}$$

$$1650\text{mm} - 100\text{mm} = 1550\text{mm} \Rightarrow e_{simulated} = \frac{50\text{mm}}{1550\text{mm}} = 3,2\% \tag{5.2}$$

These new normalised errors, $e_{simulated}$ and e_{real}, better illustrate the performance of the networks when compared to each other. There is still a difference in favour of the network trained on real A-scans; however, not to the same extent.

The remaining difference in accuracy can be explained when analysing how the A-scans from simulation compare to real-world A-scans. Training on simulated data yields a higher training accuracy because the network can conform to the given A-scans faster. When giving the network new A-scans to perform a validation test, it often tries to classify these as a depth close to the one it has trained on. This yields higher validation errors than the network trained on real traces, as these real A-scans all exhibit uniqueness beyond where the second pulse response appears. The network will thus not classify traces of almost the same depth as it has learned that other features are distinguishing them. Therefore, the validation accuracy is higher in the network trained on real-world data than the one trained with simulated A-scans. Although the networks have the same structure, the real A-scans give their network a more profound complexity because of the complexity of these real A-scans.

The accuracy could be further improved by utilising a GPR with higher frequency. With a higher frequency, the A-scan contain more detailed information

while not reaching as deep. In this case, the depth is not an issue as only depths up to 2m are considered. If the frequency were to rise, then the border between snow and substrate would be more distinguished, possibly increasing the accuracy of the ANN.

5.2 Robustness of neural network solution

With an error of 1 cm when classifying new A-scans with the neural network, it is essential to look at the network's robustness. High accuracy, such as 1 cm, is not the only criterion for a valid solution; the robustness of the solution is also essential. The A-scans used to train and validate the network are all from the same type of snow, as shown in Figure 3.8. The radar waves' propagation speed was assumed to be constant over the measured area's span; if new A-scans were measured from the snow with a different propagation speed, the accuracy of the neural network predictions could drop. The amount to which the propagation speed changes can not be too extreme, as explained in section 2.3.3 and has thus not been incorporated in this solution. However, to acquire a more robust network solution in future work, it could be advantageous also to have an input value changing depending on the propagation speed of the currently measured snow in parallel with the A-scan input.

5.3 Obstacle detection

As presented in section 4.2, the developed network cannot detect cooling pipes when only presented with A-scans. An idea for further development could be to develop a neural network that uses B-scans to detect and analyse the obstacles' response. This could be both after making a hyperbola generator for the B-scans or after. The utility of such a system would exist in the possibility to quickly identify all underlying materials, for example, in the construction field.

5.4 Viabillity of C.E.S.A.-GPR

The C.E.S.A.-GPR can not, in the proposed form, give a direct measurement of the depth of snow. It relies, like ordinary GPRs do, on knowing the propagation speed of the medium measured and applying a scale to each scan that way. These scans can later be input to a similar CNN proposed in chapter 3.3.3, where the depth can be predicted without knowing the propagation speed. It is possible to make this prediction directly and in real-time on the Arduino microcontroller such that the depth is directly available when measuring. This would require a microcontroller with a 32-bit processor, as this is a requirement of the Tensorflow lite library[54]. The currently proposed microcontroller is an Arduino Mega 2560, which supports an LCD screen. However, it has an 8-bit processor. To acquire real-time depth predictions from the C.E.S.A.-GPR, the microcontroller needs to be changed to one with a 32-bit processor. Alternatively, an additional microcontroller with a 32-bit processor could be connected to the system that gets data from the 8-bit

microcontroller and predicts the depth using Tensorflow lite. This would make the C.E.S.A.-GPR a self-contained real-time snow measuring unit.

6
Conclusion

The measuring of snow depth in real-time is a concept that is easy to grasp. Its execution, however, poses complications. Looking at ground-based solutions narrows the broad spectrum encapsulated by this topic and the number of applications and research areas. This thesis' aim, researching a solution to obtain real-time depth measurement, was reached by combining sensor solutions with a machine learning network to process the obtained data.

A ground penetrating radar was deemed the most straightforward and efficient method of obtaining reliable values regarding snow depth. It was combined with a CNN to anchor its use as a real-time solution by sending the raw pulses from the measurement to the network. An accuracy of 1 cm was reached with this method. The data from the GPR was minimally processed, and the CNN is a simple one-dimensional network. Resolving the aim of this topic with satisfying results highlights the possibility for future improvements.

Accurate data regarding snow depth is crucial for safety in many regards. These values can be used to prevent accidents for operators in the mountains or icy regions, as well as facilitate road maintenance and monitor water contents arising from snow melt. The possibility of obtaining values in real-time reinforces these fields by making information easier to obtain, read, and use, especially in time-critical fields.

The GPR used to obtain the presented result was not explicitly intended for this application due to a low working frequency. The tests performed were in controlled environments. Therefore, the possibility to improve the existing systems lies in designing a GPR suited to this application and a more robust network. Solutions to tackle snows with different characteristics should be considered as a possibility to enhance the system with additional variables. Promising results regarding snow depth measurement with a GPR and neural network and easy usage will significantly assist in several fields.

The successful integration of a GPR with a CNN to obtain real-time snow depth measurements, achieving an accuracy of 1 cm, highlights the potential for enhanced safety, efficiency, and decision-making in various fields. At the same time, future improvements in GPR design and network robustness offer promising opportunities for further advancements in this area.

Bibliography

[1] M. Dent, "Why snow costs america a fortune every year," January 2023, last accessed May 18, 2023. [Online]. Available: https://thehustle.co/why-snow-costs-america-a-fortune-every-year/

[2] Polar View, "Snow monitoring," last accessed May 18, 2023. [Online]. Available: https://polarview.org/services/snow-monitoring/

[3] T. Jonas, C. Marty, and J. Magnusson, "Estimating the snow water equivalent from snow depth measurements in the swiss alps," *Journal of Hydrology*, vol. 378, no. 1, pp. 161–167, 2009. [Online]. Available: https://www.sciencedirect.com/science/article/pii/S0022169409005848

[4] National Weather Service, "Snow measurement," last accessed May 18, 2023. [Online]. Available: https://www.weather.gov/dvn/snowmeasure

[5] Met Office, "Snow depth - weather observations," accessed: [Access Date]. [Online]. Available: https://www.metoffice.gov.uk/weather/guides/observations/snow-depth

[6] NASA, "Got snow? a citizen science initiative to measure snow depth with smartphones," last accessed May 18, 2023. [Online]. Available: https://snow.nasa.gov/sites/default/files/Got_SnowSM.pdf

[7] R. Clarke, "Magnetic properties of materials," 2008, last accessed May 16, 2023. [Online]. Available: http://info.ee.surrey.ac.uk/Workshop/advice/coils/mu/

[8] J. H. Chilton, R. A. Egler, K. L. Johnston, R. J. Mowat, P. K. Ramakrishnan, J. S. Risley, and M. G. Snyder, "Lab manual," 2012. [Online]. Available: https://www.webassign.net/labsgraceperiod/ncsuplseem2/lab_10/manual.html

[9] Online School Base, "Physics form 4 topic 1," 2023, last accessed June 1, 2023. [Online]. Available: https://www.onlineschoolbase.com/p/physics-form-4-topic-1.html

[10] M. Goettlieb and R. Pfeiffer, "Optics: The principle of least time," 2013, last accessed May 16, 2023. [Online]. Available: https://www.feynmanlectures.caltech.edu/I_26.html

[11] Testbook, "Bandwidth of a signal: Definition, formula, steps to calculate and applications," 2023, last accessed May 02, 2023. [Online]. Available: https://testbook.com/physics/bandwidth-of-a-signal

[12] C. Wolff, "Radar basics," Nov 1998, last accessed May 24. 2023. [Online]. Available: https://www.radartutorial.eu/index.en.html

[13] Techtarget, "Antenna," 2023, last accessed May 02, 2023. [Online]. Available: https://www.techtarget.com/searchmobilecomputing/definition/antenna

[14] S. G. Warren, "Optical properties of ice and snow," *Philosophical Transactions of the Royal Society A: Mathematical, Physical and Engineering Sciences*, Apr

2019. [Online]. Available: https://royalsocietypublishing.org/doi/10.1098/rsta.2018.0161

[15] J. W. Glen and J. G. Paren, "The electrical properties of snow and ice," *Journal of Glaciology*, vol. 15, no. 73, p. 15–38, 1975.

[16] S. Sugiyama, H. Enomoto, S. Fujita, K. Fukui, F. Nakazawa, and P. Holmlund, "Dielectric permittivity of snow measured along the route traversed in the japanese–swedish antarctic expedition 2007/08," *Annals of Glaciology*, vol. 51, no. 55, p. 9–15, 2010.

[17] M. Farzaneh, I. Fofana, and H. Hemmatjou, "Electrical properties of snow," *Annual Report - Conference on Electrical Insulation and Dielectric Phenomena, CEIDP*, pp. 611–614, 01 2004.

[18] C. Pielmeier and M. Schneebeli, "Developments in the stratigraphy of snow," *Surveys in Geophysics*, vol. 24, no. 5, pp. 389–416, 2003.

[19] S. Earle, *How Glaciers work*. BCcampus, 2019, ch. 16.2.

[20] P. Palanisamy, "Applied deep learning - part 1: Artificial neural networks," *Towards Data Science*, 2018. [Online]. Available: https://towardsdatascience.com/applied-deep-learning-part-1-artificial-neural-networks-d7834f67a4f6

[21] A. Shenfield and M. Howarth, "A novel deep learning model for the detection and identification of rolling element-bearing faults," *Sensors (Basel, Switzerland)*, vol. 20, 09 2020.

[22] M. Wahde, *Biologically Inspired Optimization Methods: An Introduction*. Springer, 2020.

[23] T. Raj, F. H. Hashim, A. B. Huddin, M. F. Ibrahim, and A. Hussain, "A survey on lidar scanning mechanisms," *Electronics*, vol. 9, no. 5, 2020. [Online]. Available: https://www.mdpi.com/2079-9292/9/5/741

[24] B. Behroozpour, P. A. M. Sandborn, M. C. Wu, and B. E. Boser, "Lidar system architectures and circuits," *IEEE Communications Magazine*, vol. 55, no. 10, pp. 135–142, 2017.

[25] X. Du, M. H. Ang, and D. Rus, "Car detection for autonomous vehicle: Lidar and vision fusion approach through deep learning framework," in *2017 IEEE/RSJ International Conference on Intelligent Robots and Systems (IROS)*, 2017, pp. 749–754.

[26] C. M. Albrecht, C. Fisher, M. Freitag, H. F. Hamann, S. Pankanti, F. Pezzutti, and F. Rossi, "Learning and recognizing archeological features from lidar data," in *2019 IEEE International Conference on Big Data (Big Data)*, 2019, pp. 5630–5636.

[27] L. Jones and P. Hobbs, "The application of terrestrial lidar for geohazard mapping, monitoring and modelling in the british geological survey," *Remote Sensing*, vol. 13, no. 3, 2021. [Online]. Available: https://www.mdpi.com/2072-4292/13/3/395

[28] J. S. Deems, T. H. Painter, and D. C. Finnegan, "Lidar measurement of snow depth: a review," *Journal of Glaciology*, vol. 59, no. 215, p. 467–479, 2013.

[29] A. W. Nolin, "Recent advances in remote sensing of seasonal snow," *Journal of Glaciology*, vol. 56, no. 200, p. 1141–1150, 2010.

[30] J. Edgren, "Lidar läser av snön framför pistmaskinen," Jan 2023. [Online]. Available: https://www.nyteknik.se/fordon/lidar-laser-av-snon-framfor-pistmaskinen-7043023

[31] V. A. Zhmud, N. O. Kondratiev, K. A. Kuznetsov, V. G. Trubin, and L. V. Dimitrov, "Application of ultrasonic sensor for measuring distances in robotics," *Journal of Physics: Conference Series*, vol. 1015, no. 3, p. 032189, may 2018. [Online]. Available: https://dx.doi.org/10.1088/1742-6596/1015/3/032189

[32] Y. A. Badamasi, "The working principle of an arduino," in *2014 11th International Conference on Electronics, Computer and Computation (ICECCO)*, 2014, pp. 1–4.

[33] T. G. Leighton, "What is ultrasound?" *Progress in Biophysics and Molecular Biology*, vol. 93, no. 1, pp. 3–83, 2007, effects of ultrasound and infrasound relevant to human health. [Online]. Available: https://www.sciencedirect.com/science/article/pii/S0079610706000812

[34] Z. S. Lim, "Development of high resolution snow depth sensor using ultrasonics," in *SENSORS, 2009 IEEE*, 2009, pp. 1738–1741.

[35] K. Wangdi and T. Wangmo, "2nd international conference on science, engineering and technology," 2016. [Online]. Available: http://scientec.cst.edu.bt/

[36] D. Nolan, "Brazenec thesis all - colorado state university," 2005. [Online]. Available: https://ccc.atmos.colostate.edu/pdfs/Brazenec_Thesis_ALL.pdf

[37] M. I. Skolnik, "radar," 2022, encyclopedia Brittanica, last accessed January 25, 2023. [Online]. Available: https://www.britannica.com/technology/radar

[38] M. Kirscht and C. Rinke, "3d reconstruction of buildings and vegetation from synthetic aperture radar (sar) images," in *IAPR International Workshop on Machine Vision Applications*, 1998.

[39] V. Bergonzi, "Measuring snow depth," 2021, eurac Research. [Online]. Available: https://www.eurac.edu/en/magazine/measuring-snow-depth-satellite

[40] Radiodetection, "What is ground penetrating radar (gpr)?" 2023. [Online]. Available: https://www.sensoft.ca/blog/what-is-gpr/

[41] Y. A. Sukhobok, L. R. Verkhovtsev, and Y. V. Ponomarchuk, "Automatic evaluation of pavement thickness in gpr data with artificial neural networks," *IOP Conference Series: Earth and Environmental Science*, vol. 272, no. 2, p. 022202, jun 2019. [Online]. Available: https://dx.doi.org/10.1088/1755-1315/272/2/022202

[42] A. E.-C. Tan, J. McCulloch, W. Rack, I. Platt, and I. Woodhead, "Radar measurements of snow depth over sea ice on an unmanned aerial vehicle," *IEEE Transactions on Geoscience and Remote Sensing*, vol. 59, no. 3, pp. 1868–1875, 2021.

[43] A. Benedetto, F. Tosti, L. Bianchini Ciampoli, and F. D'Amico, "An overview of ground-penetrating radar signal processing techniques for road inspections," *Signal Processing*, vol. 132, pp. 201–209, 2017. [Online]. Available: https://www.sciencedirect.com/science/article/pii/S0165168416300792

[44] USRADARinc, "How much does ground penetrating radar cost?" 2021. [Online]. Available: https://usradar.com/blog/how-much-does-ground-penetrating-radar-cost/

[45] M. Küçükdemirci and A. Sarris, "Gpr data processing and interpretation based on artificial intelligence approaches: Future perspectives for archaeological prospection," *Remote Sensing*, vol. 14, no. 14, 2022. [Online]. Available: https://www.mdpi.com/2072-4292/14/14/3377

[46] I. Giannakis, A. Giannopoulos, and C. Warren, "A machine learning-based fast-forward solver for ground penetrating radar with application to full-waveform inversion," *IEEE Transactions on Geoscience and Remote Sensing*, vol. 57, no. 7, pp. 4417–4426, 2019.

[47] C. Warren, A. Giannopoulos, and I. Giannakis, "gprmax: Open source software to simulate electromagnetic wave propagation for ground penetrating radar," *Computer Physics Communications*, vol. 209, pp. 163–170, 2016. [Online]. Available: https://www.sciencedirect.com/science/article/pii/S0010465516302533

[48] S. D. Gedney, *Yee Algorithm for Maxwell's Equations*. Cham: Springer International Publishing, 2011, pp. 39–73. [Online]. Available: https://doi.org/10.1007/978-3-031-01712-4_3

[49] E. Huber and G. Hans, "Rgpr — an open-source package to process and visualize gpr data," in *2018 17th International Conference on Ground Penetrating Radar (GPR)*, 2018, pp. 1–4.

[50] M. Paun, "Gprino," 2020, hackaday, last accessed April 27, 2023. [Online]. Available: https://hackaday.io/project/175115-gprino

[51] MathWorks, "Antenna toolbox," 2023, matlab toolbox, last accessed April 27, 2023. [Online]. Available: https://www.mathworks.com/help/antenna

[52] Bazoozoo, "Gprino antenna vivaldi style," 2023, last accessed May 17, 2023. [Online]. Available: https://imgur.com/a/zWIoyvj

[53] A. Dixit S. and S. Kumar, "A survey of performance enhancement techniques of antipodal vivaldi antenna," 2020, last accessed May 17, 2023. [Online]. Available: https://ieeexplore.ieee.org/stamp/stamp.jsp?arnumber=9017985

[54] TensorFlow, "Tensorflow lite for microcontrollers," May 2023. [Online]. Available: https://www.tensorflow.org/lite/microcontrollers

A

Appendix 1

A.1 C.E.S.A-GPR PCB schematics

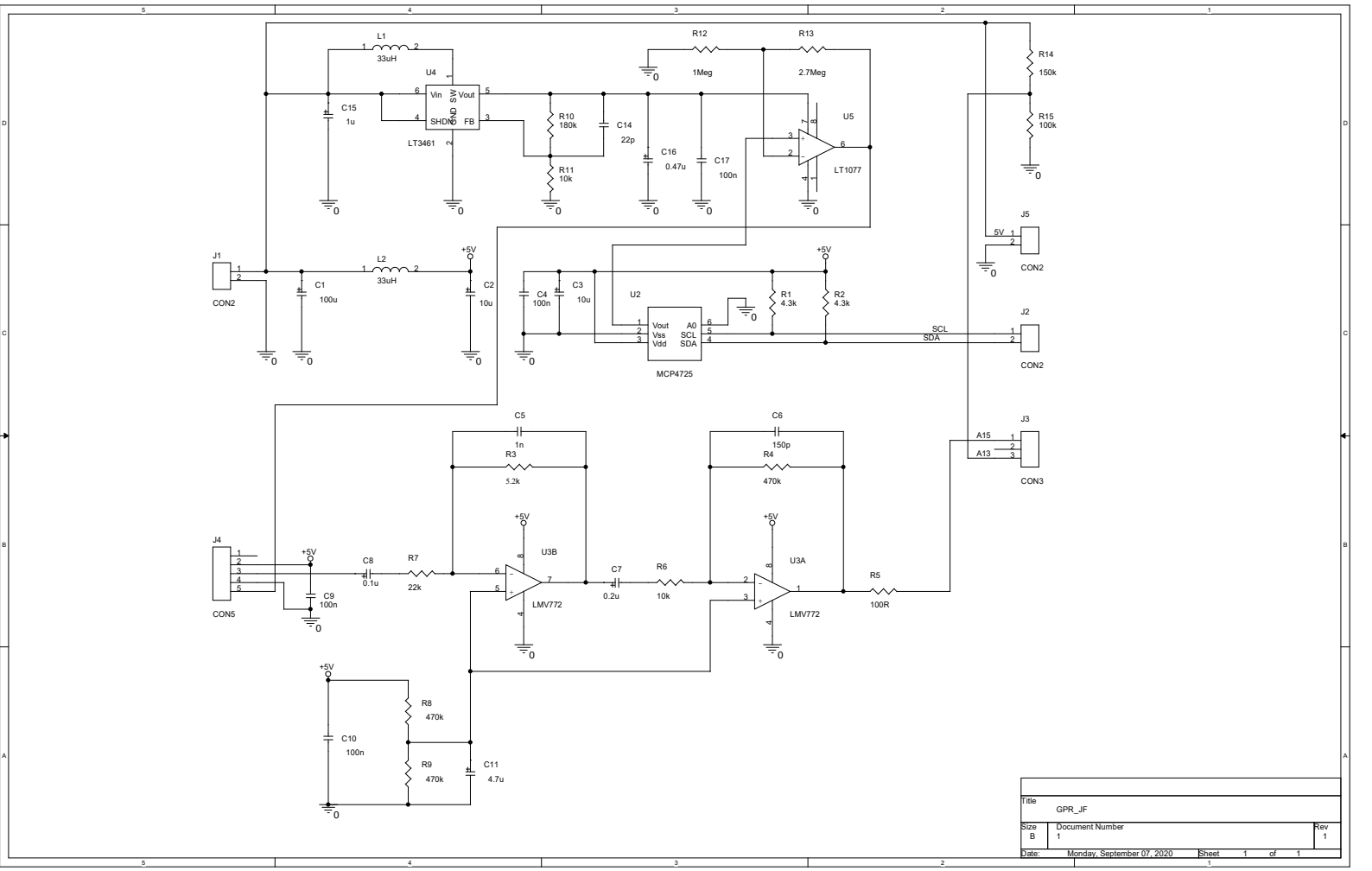

Title	GPR_JF	
Size B	Document Number 1	Rev 1
Date: Monday, September 07, 2020	Sheet 1 of 1	

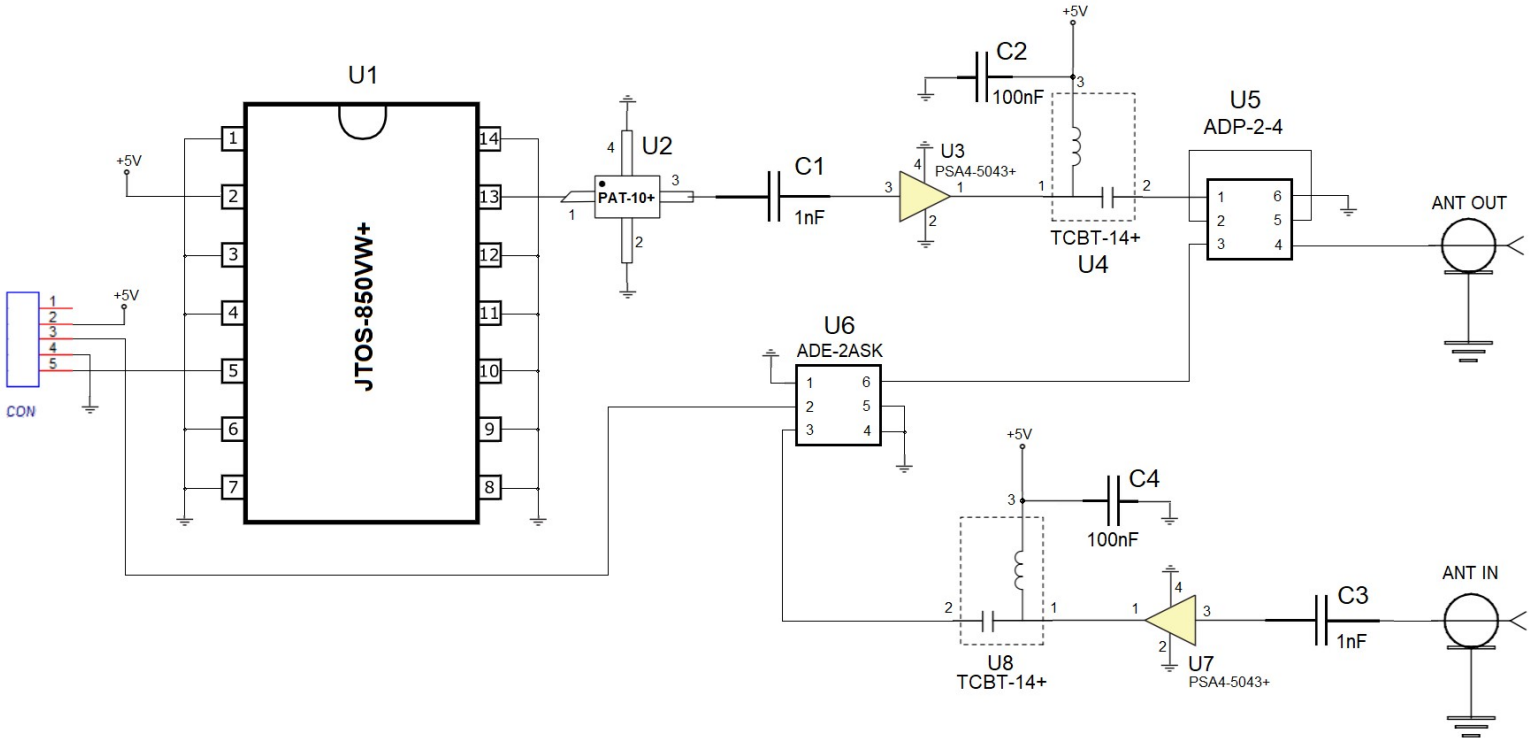
U1
JTOS-850VW+
+5V
CON
U2
PAT-10+
C1
1nF
U3
PSA4-5043+
C2
100nF
U4
TCBT-14+
U5
ADP-2-4
ANT OUT
U6
ADE-2ASK
C4
100nF
U8
TCBT-14+
U7
PSA4-5043+
C3
1nF
ANT IN

A.2 C.E.S.A-GPR Antenna design

Modelling the antenna in Matlab to print a vinyl cutout and make simulations on the antenna shape led to the following figures:

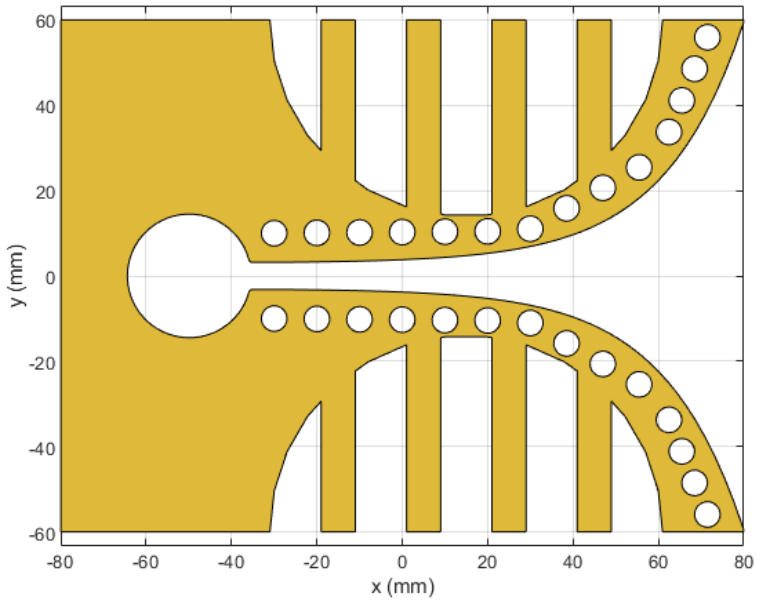

Figure A.1: Top layer of the antenna

A radial stub matching figure A.1 is designed and the schematic of the top and bottom layers is shown under:

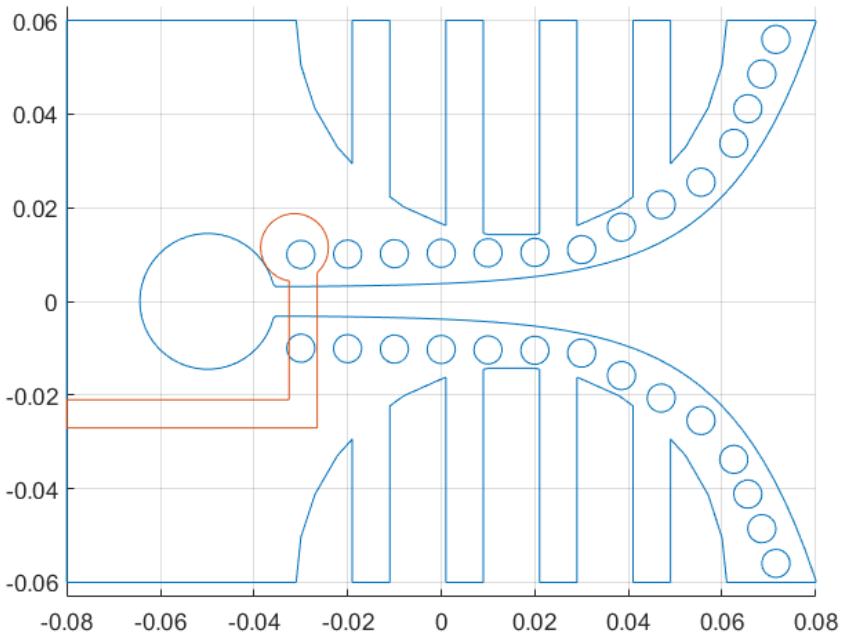

Figure A.2: Antenna schematic with top and bottom layer

DEPARTMENT OF SOME SUBJECT OR TECHNOLOGY
CHALMERS UNIVERSITY OF TECHNOLOGY
Gothenburg, Sweden
www.chalmers.se

CHALMERS
UNIVERSITY OF TECHNOLOGY